Bhaskarapillai *et al.*
Journal of Engineering and Applied Science (2024) 71:136
https://doi.org/10.1186/s44147-024-00461-3

Journal of Engineering and Applied Science

RESEARCH Open Access

Exploring the structural and electronic characteristics of phenethylamine derivatives: a density functional theory approach

Arya Bhaskarapillai[1,3], Sachidanandan Parayil[4], Jayasudha Santhamma[5], Deepa Mangalam[6] and Velupillai Madhavan Thampi Anandakumar[1,2*]

*Correspondence:
anand@vtmnsscollege.ac.in

[1] Department of Physics, Mahatma Gandhi College, Kesavadaspuram, Thiruvananthapuram 695004, Kerala, India
[2] Department of Physics, VTMNSS College, Dhanuvachapuram 695503, Kerala, India
[3] Department of Physics, University College, Palayam, Thiruvananthapuram 695034, Kerala, India
[4] Department of Forensics Science, Kerala Police Academy, Ramavarmapuram, Thrissur 680631, Kerala, India
[5] Department of Physics, HHMSPBNSS College for Women, Neeramankara, Thiruvananthapuram 695040, Kerala, India
[6] School of Sciences, Christ (Deemed to be University), Banglore 560029, Kerala, India

Abstract

Accurate structure elucidation of biologically active molecules is crucial for designing and developing new drugs, as well as for analyzing their pharmacological activity. In this study, density functional theory calculations are applied to explore the electronic structure and properties of phenethylamine derivatives, including Amphetamine, Methamphetamine, and Methylene Dioxy Methamphetamine(MDMA). The investigation encompasses various aspects such as geometry optimization, vibrational analysis, electronic properties, Molecular Electrostatic Potential analysis, and local and global descriptor analysis. Additionally, the study utilizes Natural Bond Orbital analysis and Quantum Theory of Atoms in Molecules to investigate the chemical bonding and charge density distributions of these compounds. Experimental techniques such as Fourier transform infrared (FT-IR) and Raman spectroscopic analysis are employed in the range of 4000-400 cm^{-1} and 4000-50 cm^{-1}, respectively. Theoretical vibrational analysis with Potential Energy Distribution(PED) assignments is conducted, and the resulting frequencies are compared to experimental spectral data, revealing good agreement. By correlating various structural parameters with the pharmacological activity of each derivative, computational structure elucidation aids in understanding the unique actions of phenethylamine derivatives. The obtained results offer a comprehensive understanding of the molecular behavior and properties of these drugs, facilitating the development of new drugs and therapies for addiction and related disorders.

Keywords: DFT, QAIM, Molecular graph, Critical points, Hirshfeld charges, NCI analysis, ELF

Introduction

The use of psychoactive substances for recreational and other illicit purposes is increasing tremendously. The most popular and the most threatening drugs are phenethyl amines which is a class of substances with documented psychoactive and stimulant effects [1]. According to the World Drug report 2022 of "United Nations Office on Drugs and Crime(UNODC)", Drug markets were temporarily disrupted in most parts of the world during the first phase of the COVID 19 pandemic, but there

was a quick recovery and the drug market of Phenethylamine group is still expanding especially in South-East Asia and North America [2]. Phenethylamines are a large group of structurally similar agents that include amphetamine, methamphetamine, MDMA and the cathinones. A remarkable characteristic of the phenethyl amine group is that a slight change in its structure can make drastic changes in its pharmacodynamics [3]. Amphetamine and its N-alkyl derivatives exert marked excitatory effects on the Central Nervous System [4]. The phenethyl amine group has served as the basic structure for the design and development of hundreds of amphetamine derivatives and each derivative has its own unique action profile even though their basic structure is similar.

The chemical structures of amphetamine, methamphetamine, and methylenedioxy methamphetamine (MDMA) share a common foundation: a phenyl ring with two carbon side chains and an amino group. However, subtle modifications distinguish them. Amphetamine bears an additional methyl group, while methamphetamine boasts an extra methyl group bonded to nitrogen, and MDMA incorporates an additional methylenedioxy group. These alterations significantly impact their biological behavior and interactions within the body [3]. Dopamine, norepinephrine, and serotonin serve as endogenous neurotransmitters, vital for functions such as attention, memory, emotion, reward, and movement. Amphetamine and methamphetamine boost the release and hinder the reuptake of these neurotransmitters, intensifying and prolonging stimulation of their receptors. Notably, methamphetamine surpasses amphetamine in potency and lipophilicity, facilitating easier traversal of the blood-brain barrier and achieving higher brain concentrations. Moreover, methamphetamine exhibits a longer half-life, prolonging its effects within the body. Both drugs act as substrates and inhibitors of the enzyme CYP2D6, crucial for metabolizing numerous drugs and neurotransmitters. MDMA also shares similar mechanisms. Unlike amphetamine and methamphetamine, which lack a methylenedioxy group, rendering them more selective for dopamine and norepinephrine than serotonin, MDMA's inclusion of a methylenedioxy group makes it more serotonin-selective [5].

Amphetamine, classified as an indirect sympathomimetic amine, induces sensations of alertness and euphoria, making it a common choice for recreational abuse. Despite its popularity in non-medical contexts, amphetamine exhibits therapeutic potential, particularly in treating conditions like obesity and attention deficit hyperactivity disorder (ADHD) . On the other hand, methamphetamine shares similar sympathomimetic properties with amphetamine but exerts more potent effects. Its high addictive potential is associated with numerous serious health complications upon misuse. MDMA, also known as 3,4 methylenedioxy methamphetamine, manifests both stimulant and hallucinogenic effects. As an empathogen entactogen, it fosters feelings of empathy and interpersonal closeness, alongside inducing euphoria and heightened physical energy [6]. However, it's imperative to exercise caution due to the addictive nature and severe side effects inherent in all three substances.Furthermore, these compounds are believed to interact with the opioid system, potentially augmenting pain relief. Additionally, MDMA's influence on the hypothalamic-pituitary-adrenal axis leads to increased

cortisol and prolactin levels, along with elevated levels of hormones such as oxytocin and vasopressin [7]. Consequently, molecules like amphetamine, methamphetamine, and MDMA occupy a unique space in chemical, medicinal, and pharmacological research, necessitating comprehensive exploration and careful use.

Extensive research has been conducted on the structure-activity relationships of amphetamine, methamphetamine, and MDMA, as evidenced by reports [3, 8, 9]. In 2012, Rolf Wilestone Berg et al. [10] conducted a study on the Raman optical activity and Raman spectra of amphetamine species to identify the different enantiomers of amphetamine derivatives. Similarly, in 2013, Francis Taplin et al. [11] reported spectroscopic analysis of phenethylamines for the same purpose. Recent studies have focused on the detection of amphetamine using quantum mechanical approaches [12, 13]. Despite the extensive research on the structure-activity relationships of amphetamine derivatives, there has been limited investigation using DFT techniques to correlate their quantum chemical properties and related parameters with their pharmacological activity. Density functional theory (DFT) is the most successful and promising quantum chemical approach to calculate the ground-state properties of atoms and molecules which uses a conceptually simple electron density term which depends on just three variables as compared to the more complicated and difficult to interpret electronic wave function. The density functional approach allows the calculation of the entire energy surface, the structure and related properties from knowledge of the electron density distribution alone . In this study, Quantum Theory of Atoms in Molecules(QAIM) [14] is also employed to examine the electron density distributions and reactivity sites of the molecules. This work analyses various vibrational modes of amphetamine derivatives computationally and experimentally with Potential Energy Distribution(PED) assignments. Molecular electrostatic potential (MEP) surface, Frontier molecular orbitals, Natural Bonding Orbitals, Electron Localized function, Non Covalent Interaction, Molecular graph and Reactivity descriptors have been analysed using both Density Functional Theory and Atoms in Molecular Theory using Multiwfn [15]. The above investigation at the molecular level helps to compare the various reactivity parameters of amphetamine, methamphetamine and MDMA and to correlate them with biological mechanism of action like drug-receptor interactions and the binding mechanism.

Method

Experimental

The title molecules amphetamine (1), methamphetamine (2) and 3,4-methylenedioxymethamphetamine (MDMA)(3) were analysed using FT-IR and FT-Raman techniques. The FT-IR spectra were recorded in the region 4000-400 cm^{-1} on an IR tracer FT-IR spectrometer(Shimadzu Cooperation, Japan), calibrated using a polystyrene standard. All samples were prepared using the KBr pellet method. The spectra were recorded with a scanning speed of 10 cm^{-1} per minute at a resolution of 4 cm^{-1}.

Raman spectra were recorded in the region 4000-400 cm^{-1} using a 532 nm diode laser as excitation wavelength on a Raman Spectrometer ("LabRam HR Evolution, HORIBA, Japan").

Computational details

All quantum mechanical calculations have been performed with the "Guassian-16 program" [16]. The density functional theory with the exchange correlational functional "B3LYP (three-parameter hybrid functional for the exchange part and the Lee-Yang-Parr correlational functional)" [17, 18] is used for the computational purpose. The "6-311 +G" set supplemented with two sets of diffuse functions and one set of polarization functions and augmented cc-pVTZ set have been utilized for the structural analysis [19–21]. The vibrational frequency assignments of the normal modes were carried out based on the PED calculations done with the help of the VEDA program [22, 23]. NBO analysis has been carried out in order to analyse the hyper conjugative and delocalized molecular charge interactions which depicts a clear picture of the intra molecular charge transfer of the molecules.

Quantum theory of Atoms in Molecules was applied to find out the electron density distributions of the molecules. Using Multiwfn software, the electron localized function, NBO Orbitals, Hirshfeld charge, Fukui functions and dual descriptors were analysed [24]. Various global reactivity descriptors such as chemical potential, chemical hardness, softness, electrophilicity and nucleophilicity index were calculated using finite difference approximation. All these functions help to find out the reactive sites of the molecule [25, 26] and to categorize these molecules based on reactivity [27, 28].

Results and discussion

Geometrical optimization

The molecular structure of the compounds 1, 2 and 3 in the ground state have been optimized using "Gaussian-16" utilizing Density functional theory with "B3LYP functional" and "6-311+G(2d,p)/cc-pVTZ basis set". The optimized geometries are displayed in Fig. 1. The values of bond length, bond angle and dihedral angles were compared with the experimentally reported values and found consistent. The thermodynamic parameters of the compound such as total thermal energy, the rotational constants and the dipole moment values obtained from B3LYP/6-311+ G(2d,p) basic sets for the molecules under study are shown in Table 1.

Frontier molecular orbitals (*FMO*)

The "Frontier molecular Orbitals-HOMO and LUMO" determines the chemical reactivity of the molecules [29]. The energy of "Highest Occupied Molecular Orbital(HOMO)" determines the electron giving capacity which characterizes nucleophilic component and "Lowest Unoccupied Molecular Orbital(LUMO)" energy describes the electron accepting ability which characterizes electrophilic component [30]. The energy difference between HOMO and LUMO is called energy gap which is a critical parameter in determining the chemical stability of a molecule and eventual charge transfer interactions within a molecule.

Figure 2 displays the 3D plots of the frontier orbitals, along with their corresponding energy values. The HOMO of amphetamine shows greater contribution from the states of the NH_2 group compared to the phenyl group, while the opposite is true for the LUMO. In the case of methamphetamine, the phenyl group does not contribute

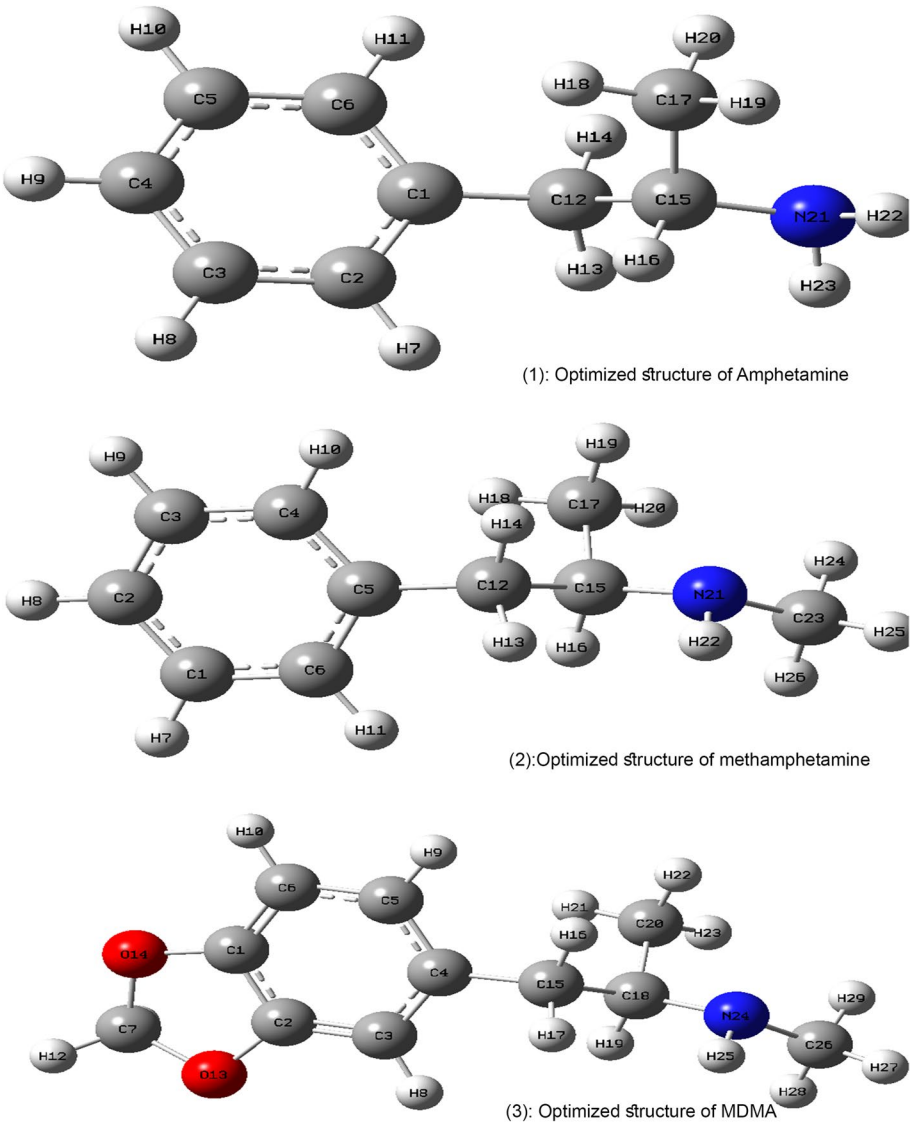

Fig. 1 The optimized structure of amphetamine(1), methamphetamine(2) and MDMA(3)

to the HOMO formation, and NH_2 does not contribute to the LUMO. This suggests that, for both amphetamine and methamphetamine, the N atom acts as a favorable site for electron-deficient groups. However, for MDMA, the NH_2 group does not contribute to either the HOMO or LUMO, possibly due to the oxygen substitutions at meta and para positions of the phenyl group.

Furthermore, the HOMO-LUMO energy gap was calculated for the three molecules, resulting in values of 6.2162, 5.760, and 5.3351 eV for amphetamine, methamphetamine, and MDMA, respectively. MDMA has the smallest HOMO-LUMO energy gap, indicating enhanced intra-molecular charge transfer interactions which may potentially influence its biological activities.

Table 1 The thermodynamic parameters calculated using B3LYP/6-311+G(2d,p) set

Thermodynamic parameters	amphetamine	methamphetamine	MDMA
SCF energy (Hartree)	-405.6638	-444.9783	-633.5652
Total thermal energy (($Kcal.mol^{-1}$)	132.68	151.32	162.23
Vibrational energy (($Kcal.mol^{-1}$)	130.903	149.354	160.448
Zero point Vibrational energy ($Kcal.mol^{-1}$)	126.4931	144.1054	153.818
Heat capacity at constant volume ($cal.mol^{-1}K^{-1}$)	37.924	42.469	50.767
Entropy ($\left(cal.mol^{-1}K^{-1}\right)$	97.708	104.905	116.465
Rotational Constants (GHz)			
A	3.114	2.8593	1.8052
B	0.725	0.5432	0.313
C	0.671	0.5057	0.2944
Dipole moment (Debye)			
μ_x	-0.3081	0.0460	0.3201
μ_y	0.9881	-0.8819	-1.0668
μ_z	-0.6947	-0.2317	0.3349
μ_{Total}	1.2466	0.9130	1.1631

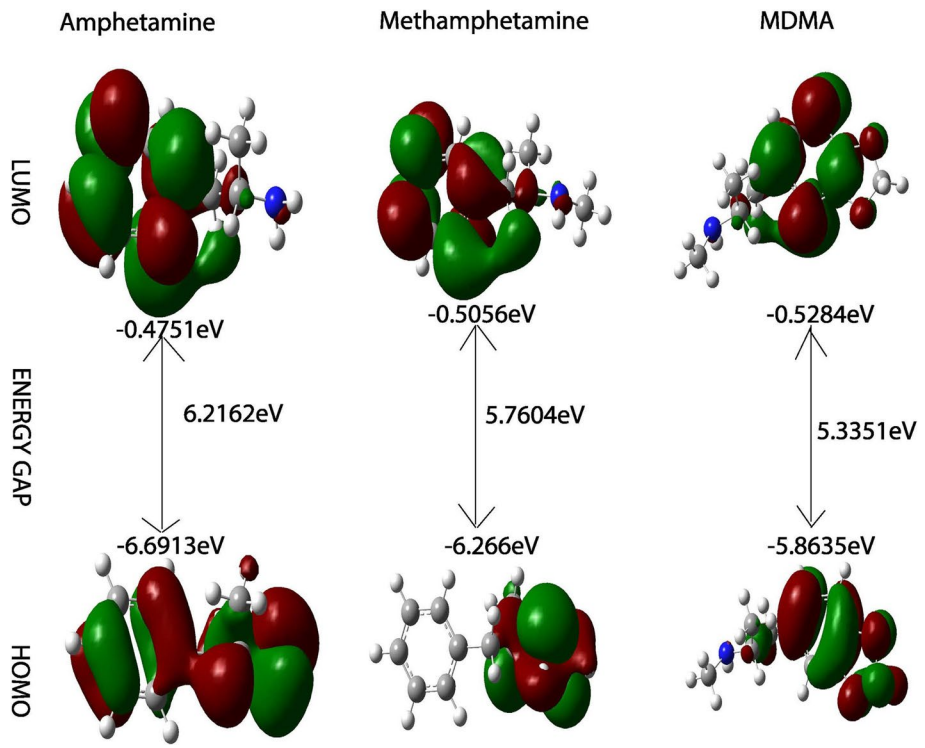

Fig. 2 Frontier orbitals

Global reactivity descriptors

The global reactivity descriptors such as "chemical hardness(η), softness(S), Chemical potential(μ), electronegativity(χ) and electrophilicity index(ω)" are important parameters for understanding the reactivity and stabilty of molecular systems [31] . The

global reactivity descriptors of the title molecules were calculated using B3LYP/6-311+G(2d,p) basic set with finite difference approximations. The values were then verified with those obtained through Multiwfn and found to be in agreement.

The "hardness" of the molecule is;

$$\eta = \frac{I - A}{2} \tag{1}$$

The "softness" of the molecule is;

$$S = \frac{1}{2\eta} \tag{2}$$

The "chemical potential" is given as;

$$\mu = -\frac{I + A}{2} \tag{3}$$

The "electronegativity" is expressed as;

$$\chi = \frac{I + A}{2} \tag{4}$$

The "electrophilicity index" of the molecule is;

$$\omega = \frac{\mu^2}{2\eta} \tag{5}$$

where I "ionization potential" and A "electron affinity" which are calculated using delta SCF method [32].

$$I = E(N-1) - E(N) \tag{6}$$

$$E = E(N) - E(N+1) \tag{7}$$

where "$E(N), E(N-1) and E(N+1)$" are the energies of "N, N-1 and N+1" eletron systems.

Electrons flow from regions of high chemical potential to regions of low chemical potential until the electronic chemical potential is constant throughout the molecule. Hence μ can be interpreted as a measure of the tendency of electrons to escape from a system. As the chemical potential becomes more negative, it becomes increasingly difficult for an electron to be lost. It is considered as negative of the Mulliken electronegativity [33]. Hardness fundamentally signifies the resistance to deformation of the electron cloud of the atoms, ions or molecules under small perturbation generated during the process of chemical reaction. If the electron cloud is strongly held by the nucleus, the chemical species is 'hard' but if the electron cloud is loosely held by the nucleus, the system is 'soft' [34, 35]. Hardness and softness are a useful concept for understanding the behaviour of chemical systems. Soft molecules will be more polarizable than hard molecules [36, 37]. Electrophilicity index is a measure of the stabilization energy when the system gets saturated by electrons. A reactive nucleophile

is characterized by a lower value of ω, while higher values indicate the presence of a good electrophile [24].

These descriptors have importance in rational drug design. However, biological systems present a collocation of simple interactions within a complex environment. Molecular descriptors are computed within an in silico framework where the dynamic roles of molecules are not fully considered. Notably, in certain instances, the transient metabolic by-products of a drug exert significant influence on its activity. Consequently, the holistic activity of a drug often arises from the cumulative effects of these individual entities. In such cases the overall activity can be predicted only after calculating the descriptors of each molecule , and it makes the system more complex. Though drug design facilitated by molecular descriptors, serves as a valuable tool for scrutinizing vast molecular libraries to identify potential candidates or for enhancing activity of existing molecules [38].

The electron affinity, ionization potential, and global reactivity descriptors of the title molecules were computed, and the results are presented in Table 2. Based on the findings, MDMA is the softest molecule among the three, as confirmed by its lowest energy gap and ionization energy. Additionally, MDMA has the lowest LUMO energy, which makes it the best electron donor. Furthermore, MDMA has the lowest chemical hardness value, making it the most reactive among the three. Therefore, the order of decreasing reactivity among the molecules is MDMA > Methamphetamine > Amphetamine. Moreover, the lower value of electrophilicity index ω suggests that the molecules exhibit good nucleophilic behavior. Furthermore, these molecular descriptors have much significance in the pharmacological activity , and they are used in quantitative structure-activity relationship(QSAR) studies and drug design. The dipole moment and polarizability represent information about charge distribution within the molecule which affect solvation and membrane permeability. The ionization potential and electron affinity provide information regarding the molecule's stability, which could also be reflected in the drug's metabolism [39]. According to studies in the literature, a decrease in polarity and an

Table 2 Calculated values of ionization potential, electron affinity and global reactivity descriptors of title molecules using B3LYP/6-311+G(2d, p) method

Parameters	Values		
	amphetamine	**Methamphetamine**	**MDMA**
Ionization potential (I) (eV)	8.084	7.59	7.13
Electron Affinity(A) (eV)	-0.8976	-0.7586	-0.71
Chemical Hardness (η)	4.4903	4.1729	3.9213
Chemical Softness(s)	0.1113	0.1198	0.1275
Chemical Potential (μ)	-3.5929	-3.4143	-3.2113
Electronegativity (χ)	3.5929	3.4143	3.2113
Electrophilicity Index (ω)	1.4374	1.3968	1.3149
E_{LUMO} (eV)	-0.4751	-0.5056	-0.5284
E_{HOMO} (eV)	-6.6913	-6.266	-5.8635
Energy Gap (E_g) (eV)	6.2162	5.760	5.3351
Dipole moment (μ)	1.247	0.913	1.163
Polarizability (α)	115.368	128.298	147.334

increase in polarizability, along with a greater ability for hydrogen bonding, significantly reduce brain penetration [39]. Consequently, Methamphetamine and MDMA exhibit higher brain penetration compared to Amphetamine, consistent with experimental findings. The electron affinity which is used for the investigation of optimal bioavailability and ionization potential which is related to the blood-brain barrier permeation. Among the three, MDMA has the lowest ionization potential, reflecting its high blood-brain barrier penetration ability. Furthermore, dipole moments of these molecules are low and close with each other and they have comparatively small size. Thus they have a good capacity to penetrate the blood brain barrier [40]. Binding to an active pocket of a receptor depends on the electronic structure of the ligand, with a significant contribution from dipole moment and polarizability [41]. This is because the electrostatic field generated by the receptor would strongly interact with molecules that have a higher dipole moment or polarizability.

Electron Localization Function (ELF) and NCI analysis

"Electron Localization Function (ELF)" is an alternative method for mapping "electron pair probability" in many-electron systems. The pair probability is a complex six-dimensional function that is difficult to analyze visually. ELF simplifies this by focusing on the spherically averaged local behavior of the pair probability as a function of a reference point. ELF is a powerful tool that helps to identify the location of atomic shell and core, binding, and lone electron pairs in atomic and molecular systems [42]. It provides insight into the atomic shell structure, type of chemical bonding, and verification of charge-shift bonds. A high ELF value indicates that electrons are highly localized, which suggests the presence of a covalent bond, a lone pair, or inner shells of the atom. The degree of electron localization directly relates to the confinement of electrons in the domain [43].

"Non-covalent interactions" are a type of interactions that play a crucial role in various chemical processes, such as the chemical interaction between a protein and a drug, and a catalyst and a substrate [44]. Although they are weaker than covalent bonds, their cumulative effect can be significant, resulting in the stabilization of molecules and complex structures. It is essential to understand the nature and strength of non-covalent interactions to develop new drugs and materials that can interact efficiently with their target molecules or systems.

A plot of NCI together with ELF is shown in Fig. 3 which can reveal both covalent and non-covalent interactions simultaneously. Both analysis have been done using Multiwfn and VMD [45]. The red colored region of the ELF map represents highest ELF value which indicates the presence of a covalent bond or a lone pair and the violet region represents lowest ELF. Both maps show the presence of a bond attractor between the core attractors which indicates a shared electron attraction. Hydrogen has no core attractor and large domain around hydrogen indicates the presence of more negative character and high electron localization. In the NCI analysis map, the red colour region at the centre of benzene ring represents strong repulsion region due to steric interaction. In MDMA, there is two steric interaction region corresponding two "ring critical points". The green colour region represents the vdW interction region where the electron density is minimum.

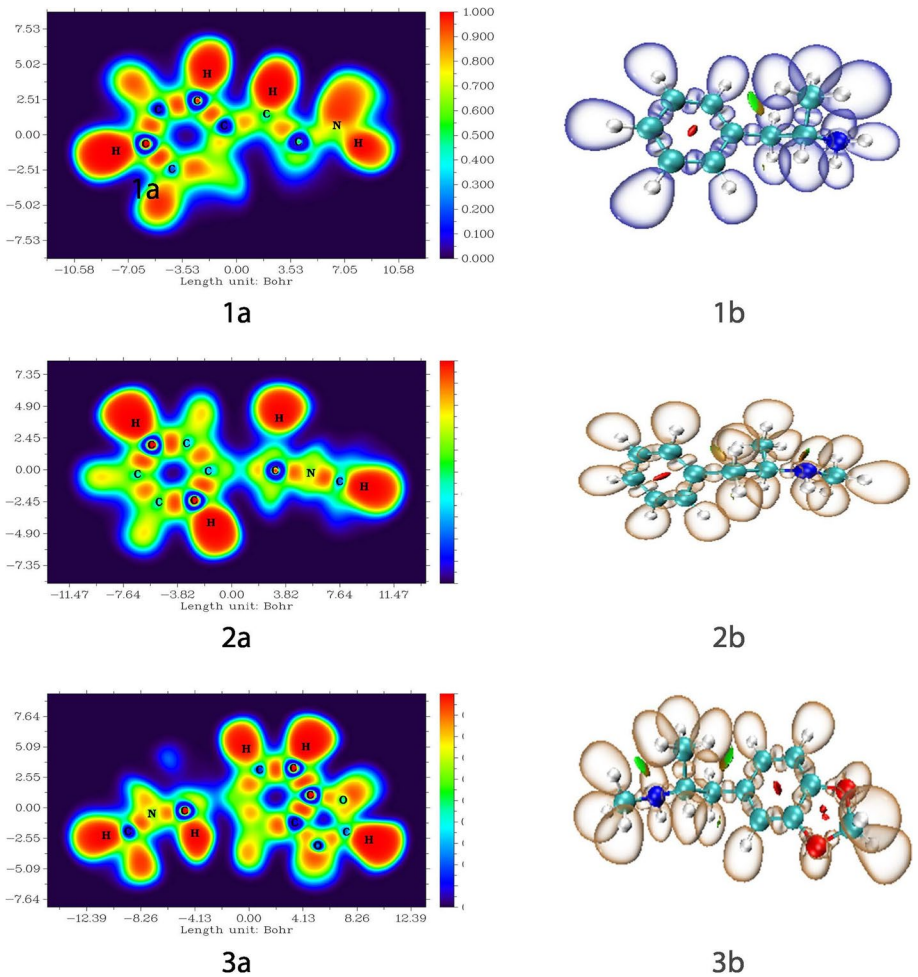

Fig. 3 Electron Localized function and NCI analysis of amphetamine [1(**a**), 1(**b**)], methamphetamine [2(**a**), 2(**b**)] and MDMA [3(**a**), 3(**b**)] plotted using Multiwfn and VMD

Amphetamine exhibits a single weak interaction region, whereas methamphetamine and MDMA display two weak interaction regions.

Molecular graph and critical points

Quantum theory of atoms in molecules (QTAIM) is a powerful theoretical framework for understanding the electronic structure of molecules. Within this framework, molecular graphs are constructed based on the distribution of electron density within the molecule [14]. Molecular graph refers to the set of bond paths that connect the nuclei of atoms within a molecule's equilibrium geometry, along with the corresponding critical points. In the context of QTAIM, as referenced by R.F.W Bader [15] in his article, "a critical point (CP) is a point in space where the first derivatives of the electron density vanish.

At critcal points

$$\nabla\rho = \hat{\imath}\frac{\partial\rho}{\partial x} + \hat{\jmath}\frac{\partial\rho}{\partial y} + \hat{z}\frac{\partial\rho}{\partial k} = \vec{0} \tag{8}$$

where the zero vector signifies that each individual derivative in the gradient operator, ∇ is zero and not just their sum. These critical points include nuclear critical points,bond critical points, ring critical points and cage critical points which are determined using mathematical algorithms that are based on the laws of quantum mechanics. The number and type of critical points that can coexist in a molecule or crystal follow a strict topological relationship which states that:

$$n_{NCP} - n_{BCP} + n_{RCP} - n_{CCP} = 1 \tag{9}$$

for isolated molecule where n denotes the number of the sub-scripted type of CP. The equality is known as the Poincare'–Hopf relationship (PH) and applies for isolated finite systems such as a molecule."

Figure 4 displays the molecular graphs of the title molecules. In the figure, blue circles indicate nuclear critical points, orange circles represent bond critical points, and yellow circles denote ring critical points. Amphetamine comprises 23 nuclear critical points, 23 bond critical points, and one ring critical point. Methamphetamine, on the other hand, features 26 nuclear critical points, 26 bond critical points, and one ring critical point. Finally, MDMA has 29 nuclear critical points, 30 bond critical points, and two ring critical points.

Hirshfeld charge and local reactivity descriptors

"Fukui Function" proposed by Parr and Yang in 1984, is one of the most important local reactivity descriptor to model chemical reactivity and site selectivity. Large values of 'f' at a site favor reactivity of that site [33]. "Conceptual Density Functional Theory" is applied to calculate the Hirshfeld Charge and Local reactivity descriptors using Multiwfn. According to Parr et al., "Fukui function is defined as the change of electron density $\rho(r)$ at each point r when the total number of electrons is changed or as the sensitivity of chemical potential μ of a system to an external perturbation at particular point r".

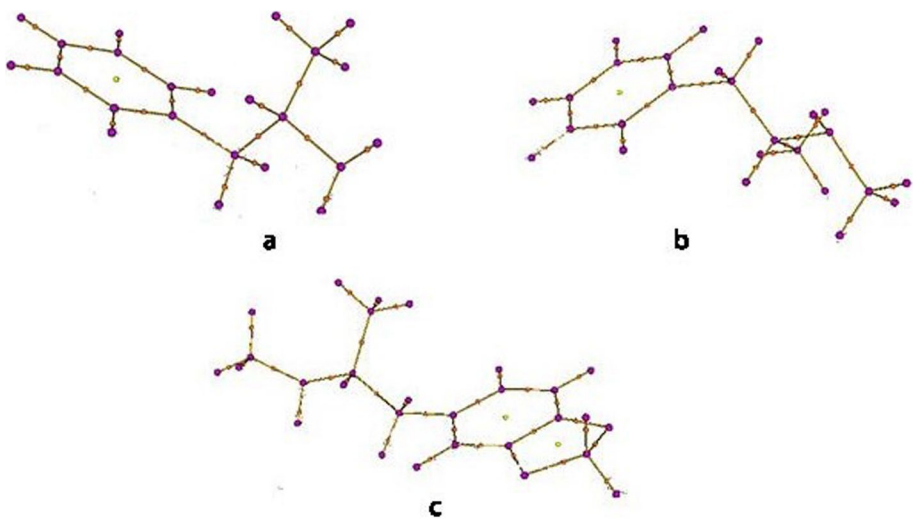

Fig. 4 Molecular graph of amphetamine (**a**), methamphetamine (**b**) and MDMA (**c**)

$$f(r) = \left(\frac{\partial \rho(r)}{\partial(N)}\right)_{v(r)} or f(r) = \left(\frac{\partial \mu}{\partial(v(r))}\right)_N \tag{10}$$

Because of its derivative discontinuity, Fukui function is often calculated approximately using finite difference method as follows [46]

$$f_-(r) = \rho_N(r) - \rho_{N-1}(r) = \rho^{Homo}(r) \tag{11}$$

$$f_+(r) = \rho_{N+1}(r) - \rho_N(r) = \rho^{Lumo}(r) \tag{12}$$

$$f_0(r) = \frac{f_-(r) + f_+(r)}{2} = \frac{\rho^{Homo}(r) + \rho^{Lumo}(r)}{2} \tag{13}$$

$\rho_N(r), \rho_{N-1}(r)$ and $\rho_{N+1}(r)$ represent separately the electron densities of the system with N, N-1 and N+1 electrons. $\rho^{Homo}(r)$ and $\rho^{Lumo}(r)$ are the electron densities of HOMO and LUMO, respectively. A large value of fukui function at a site favors reactivity of that site [33] and hence it is used to identify the electrophilic and nucleophilic attack sites of a molecule. When integrating the above equation for individual atoms in a molecule, the resulting "Condensed Fukui Function (CFF)" [47] can provide a more convenient method for predicting reaction sites within the molecule. For a given atom "K" in the molecule, three types of Condensed Fukui Functions can be defined based on the electron transfer involved [33].

For nucleophilic attack,

$$f_k^+(r) = q_k(N+1) - q_k(N) \tag{14}$$

For electrophilic attack,

$$f_k^-(r) = q_k(N) - q_k(N-1) \tag{15}$$

For radial attack,

$$f_k^0(r) = \frac{1}{2}[q_k(N+1) - q_k(N-1)] \tag{16}$$

where q_k is the gross electronic population of atom k in the molecule.

Dual descriptor (DD) was proposed by Morell et al. in 2005 [48] which is a more convenient tool to be used for predicting the reactive sites as it can reveal both types of reactive sites simultaneously.

$$f(r) = \left(\frac{\partial \eta(r)}{\partial(V(r))}\right)_N or f(r) = \left(\frac{\partial f(r)}{\partial(N)}\right)_{V(r)} \tag{17}$$

where η is the chemical hardness of the system. Using the same approximation as in the Fukui function, Condensed Dual Descriptor (CDD) can be expressed as follows:

$$f^2(r) = f^+(r) - f^-(r) = \rho^{Lumo}(r) - \rho^{HOmo}(r) \tag{18}$$

The dual descriptor $f^2(r)$ will be positive in electrophilic regions where $\rho^{Lumo}(r)$ dominates and negative in nucleophilic regions where $\rho^{Homo}(r)$ dominates. The calculated values of Hirshfeld charges, condensed Fukui function and Dual Descriptor are shown in the Tables 3, 4 and 5.

The values of condensed fukui functions and dual descriptor indicates that for all the three molecules,the region around nitrogen are the most reactive site for nucleophilic attack. For amphetamine, the region around 21N, 17C, 20H, 12C, 6C, 16H, 5C, 4C and 1C are the reactive sites for nucleophilic attack and nucleophilicity decreases in the order $21N > 17C > 20H > 12C > 6C > 4C > 5C > 16H > 1C$. For methamphetamine, nucleophilicity decreases in the order $21N > 1C > 4C > 22H > 5C > 16H > 23C > 2C > 24H > 15C > 19H$ and for MDMA, the nucleophilicity decreases in the order $24N > 14O > 13O > 1C > 5C > 4c > 19H > 18C > 23H > 21H > 20C$.

Molecular electrostatic potential analysis

The molecular electrostatic potential map illustrates the charge distribution of a molecule three-dimensionally which is a critical factor for understanding the reactive sites of electrophilic and nucleophilic attack of a molecule. This map also help to understand the different polar regions of a molecule as well as the net electrostatic

Table 3 Hirshfeld charges, condensed Fukui functions and dual descriptors of amphetamine

atom	Hirshfeld charges			Condensed Fukui Functions			CDD
	q(N)	q(N+1)	q(N-1)	f-	f+	f0	
1(C)	0.0079	-0.0059	0.0451	0.0372	0.0138	0.0255	-0.0234
2(C)	-0.0440	-0.0667	-0.0367	0.0072	0.0227	0.0150	0.0155
3(C)	-0.0418	-0.0757	-0.0139	0.0279	0.0339	0.0309	0.0060
4(C)	-0.0451	0.0171	0.0505	0.0956	-0.0622	0.0167	-0.1577
5(C)	-0.0413	-0.0149	0.0523	0.0936	-0.0264	0.0336	-0.1199
6(C)	-0.0413	-0.0338	0.0591	0.1005	-0.0075	0.0465	-0.1080
7(H)	0.0359	-0.0646	0.0317	-0.0042	0.1005	0.0481	0.1047
8(H)	0.0389	-0.0726	0.0463	0.0073	0.1115	0.0594	0.1042
9(H)	0.0389	-0.0389	0.0662	0.0273	0.0778	0.0525	0.0505
10(H)	0.0393	-0.1309	-0.0708	-0.1101	0.1702	0.0300	0.2803
11(H)	0.0378	-0.2249	-0.0311	-0.0689	0.2627	0.0969	0.3316
12(C)	-0.0501	-0.0055	0.0520	0.1021	-0.0447	0.0287	-0.1468
13(H)	0.0295	-0.0785	0.0028	-0.0266	0.1080	0.0407	0.1347
14(H)	0.0308	-0.0297	0.0634	0.0326	0.0605	0.0466	0.0279
15(C)	0.0256	-0.0836	0.0073	-0.0182	0.1092	0.0455	0.1274
16(H)	0.0128	-0.0115	0.0777	0.0649	0.0243	0.0446	-0.0406
17(C)	-0.0905	-0.0221	0.0453	0.1358	-0.0684	0.0337	-0.2042
18(H)	0.0294	-0.0333	0.0591	0.0297	0.0627	0.0462	0.0330
19(H)	0.0276	-0.0372	0.0499	0.0223	0.0649	0.0436	0.0426
20(H)	0.0279	0.0253	0.1521	0.1242	0.0025	0.0634	-0.1217
21(N)	-0.2042	0.0206	0.1461	0.3504	-0.2249	0.0627	-0.5752
22(H)	0.0886	-0.0122	0.0715	-0.0171	0.1008	0.0419	0.1179
23(H)	0.0876	-0.0093	0.0743	-0.0133	0.0969	0.0418	0.1102

Table 4 Hirshfeld charges, condensed Fukui functions and dual descriptors of methamphetamine

atom	Hirshfeld charges			Condensed Fukui Functions			CDD
	q(N)	q(N+1)	q(N-1)	f-	f+	f0	
1(C)	-0.0414	-0.0750	0.0185	0.0599	0.0336	0.0467	-0.0263
2(C)	-0.0446	-0.0841	0.0355	0.0801	0.0395	0.0598	-0.0406
3(C)	-0.0410	-0.0734	-0.0047	0.0363	0.0324	0.0344	-0.0039
4(C)	-0.0410	-0.0631	0.0098	0.0507	0.0221	0.0364	-0.0287
5(C)	0.0084	-0.0013	0.0563	0.0479	0.0097	0.0288	-0.0382
6(C)	-0.0434	-0.0704	-0.0184	0.0250	0.0270	0.0260	0.0020
7(H)	0.0391	-0.0336	0.0711	0.0320	0.0728	0.0524	0.0408
8(H)	0.0391	-0.0303	0.0749	0.0358	0.0694	0.0526	0.0337
9(H)	0.0395	-0.0290	0.0674	0.0279	0.0685	0.0482	0.0405
10(H)	0.0379	-0.0096	0.0637	0.0258	0.0475	0.0367	0.0218
11(H)	0.0362	-0.0605	0.0583	0.0221	0.0967	0.0594	0.0746
12(C)	-0.0487	-0.0679	-0.0352	0.0135	0.0193	0.0164	0.0058
13(H)	0.0291	-0.0320	0.0491	0.0200	0.0610	0.0405	0.0410
14(H)	0.0312	0.0007	0.0548	0.0237	0.0304	0.0270	0.0067
15(C)	0.0262	0.0171	0.0490	0.0228	0.0090	0.0159	-0.0138
16(H)	0.0121	-0.0187	0.0581	0.0460	0.0307	0.0384	-0.0153
17(C)	-0.0918	-0.1082	-0.0794	0.0125	0.0163	0.0144	0.0039
18(H)	0.0279	0.0146	0.0410	0.0131	0.0133	0.0132	0.0002
19(H)	0.0270	0.0063	0.0483	0.0212	0.0208	0.0210	-0.0004
20(H)	0.0282	0.0093	0.0453	0.0172	0.0189	0.0180	0.0017
21(N)	-0.1488	-0.1658	0.0095	0.1583	0.0169	0.0876	-0.1414
22(H)	0.0875	0.0194	0.1419	0.0545	0.0681	0.0613	0.0136
23(C)	-0.0458	-0.0826	-0.0064	0.0394	0.0368	0.0381	-0.0026
24(H)	0.0302	0.0156	0.0616	0.0314	0.0146	0.0230	-0.0169
25(H)	0.0333	-0.0265	0.0654	0.0321	0.0598	0.0459	0.0277
26(H)	0.0142	-0.0367	0.0645	0.0503	0.0509	0.0506	0.0006

effect caused due to total charge distribution [26]. As reported by W J Hehre [25], "the molecular electrostatic potential at a point in the space can be expressed as

$$V(r) = \sum_{A} \frac{Z_A}{|R_A - r|} - \int \frac{\rho(r)dr'}{\left|\vec{r'} - \vec{r}\right|} \tag{19}$$

where Z_A is the charge on nucleus A located at R_A and $\rho(r)$ is the electron density function. The first and second terms represent the contribution by the nuclei and electrons of the molecule to the electrostatic potential produced at the point r". The electron density surface mapped with electrostatic potential reveals the shape, size, charge density distribution and site of chemical reactivity of a molecule [49–51].

A high electrostatic potential represents the relative lack of electrons and a low electrostatic potential indicates the abundance of electrons at that region. The surface is color coded according to the variation in the electrostatic potential. The lowest electrostatic potential is indicated by red, while the highest is shown by blue, and the zero electrostatic potential is represented by green in the figures. The electrostatic potential increases in the order red < orange < yellow < green < blue. In Fig. 5, the total electron density surface mapped with the electrostatic potential and the contour map of the

Table 5 Hirshfeld charges, condensed Fukui functions and dual descriptors of MDMA

atom	Hirshfeld charges			Condensed Fukui Functions			CDD
	q(N)	q(N+1)	q(N-1)	f-	f+	f0	
1(C)	0.0466	0.0154	0.1047	0.0581	0.0312	0.0447	-0.0269
2(C)	0.0494	0.0247	0.0903	0.0409	0.0247	0.0328	-0.0162
3(C)	-0.0561	-0.1025	-0.0388	0.0173	0.0464	0.0319	0.0291
4(C)	0.0006	-0.0174	0.0376	0.0370	0.0180	0.0275	-0.0190
5(C)	-0.0503	-0.0720	0.0027	0.0530	0.0217	0.0373	-0.0312
6(C)	-0.0538	-0.1017	-0.0216	0.0322	0.0479	0.0401	0.0156
7(C)	0.1147	0.0754	0.1496	0.0349	0.0394	0.0371	0.0045
8(H)	0.0452	-0.0229	0.0665	0.0214	0.0681	0.0447	0.0467
9(H)	0.0377	0.0108	0.0627	0.0250	0.0269	0.0260	0.0019
10(H)	0.0485	0.0093	0.0769	0.0284	0.0392	0.0338	0.0108
11(H)	0.0393	-0.0121	0.0794	0.0401	0.0514	0.0457	0.0113
12(H)	0.0528	-0.0200	0.0798	0.0270	0.0728	0.0499	0.0458
13(O)	-0.1409	-0.1608	-0.0856	0.0553	0.0200	0.0376	-0.0354
14(O)	-0.1413	-0.1652	-0.0716	0.0697	0.0240	0.0468	-0.0457
15(C)	-0.0488	-0.0652	-0.0377	0.0111	0.0163	0.0137	0.0052
16(H)	0.0314	0.0080	0.0471	0.0157	0.0234	0.0196	0.0077
17(H)	0.0282	-0.0403	0.0472	0.0190	0.0686	0.0438	0.0496
18(C)	0.0255	0.0207	0.0514	0.0259	0.0048	0.0153	-0.0211
19(H)	0.0115	-0.0020	0.0477	0.0362	0.0135	0.0249	-0.0227
20(C)	-0.0921	-0.1037	-0.0780	0.0141	0.0116	0.0128	-0.0025
21(H)	0.0271	0.0166	0.0408	0.0137	0.0105	0.0121	-0.0032
22(H)	0.0271	0.0071	0.0405	0.0134	0.0199	0.0167	0.0065
23(H)	0.0278	0.0087	0.0505	0.0226	0.0192	0.0209	-0.0035
24(N)	-0.1488	-0.1618	-0.0325	0.1162	0.0131	0.0647	-0.1032
25(H)	0.0874	0.0099	0.1380	0.0505	0.0775	0.0640	0.0270
26(C)	-0.0459	-0.0814	-0.0147	0.0312	0.0355	0.0334	0.0043
27(H)	0.0333	-0.0353	0.0636	0.0303	0.0685	0.0494	0.0382
28(H)	0.0142	-0.0344	0.0553	0.0411	0.0486	0.0448	0.0074
29(H)	0.0300	0.0039	0.0483	0.0182	0.0262	0.0222	0.0079

electrostatic potential are shown. For amphetamine and methamphetamine, the lowest electrostatic potential region was located over the nitrogen atom due to the presence of lone pair of electrons, while the positive potential sites were around the hydrogen atoms. For MDMA, the lowest electrostatic potential region was found over the nitrogen and oxygen atoms. The negative potential regions of the molecule were expected to be the sites of nucleophilic attack, while the positive potential regions were expected to be the sites of electrophilic attack. The green area over the aromatic ring represents a zero electrostatic potential region, leaving a more electrophilic region in the plane of the hydrogen atoms.

NBO analysis

NBO analysis is an efficient tool in molecular structure studies for analysing the hybridization, charge transfer and conjugative interaction effects [52, 53]. NBO analysis has been done using NBO program implemented in the Guassian-16 package with basic set B3LYP/6-311+G(2d,p). The NBO program is designed to analyze the many-electron

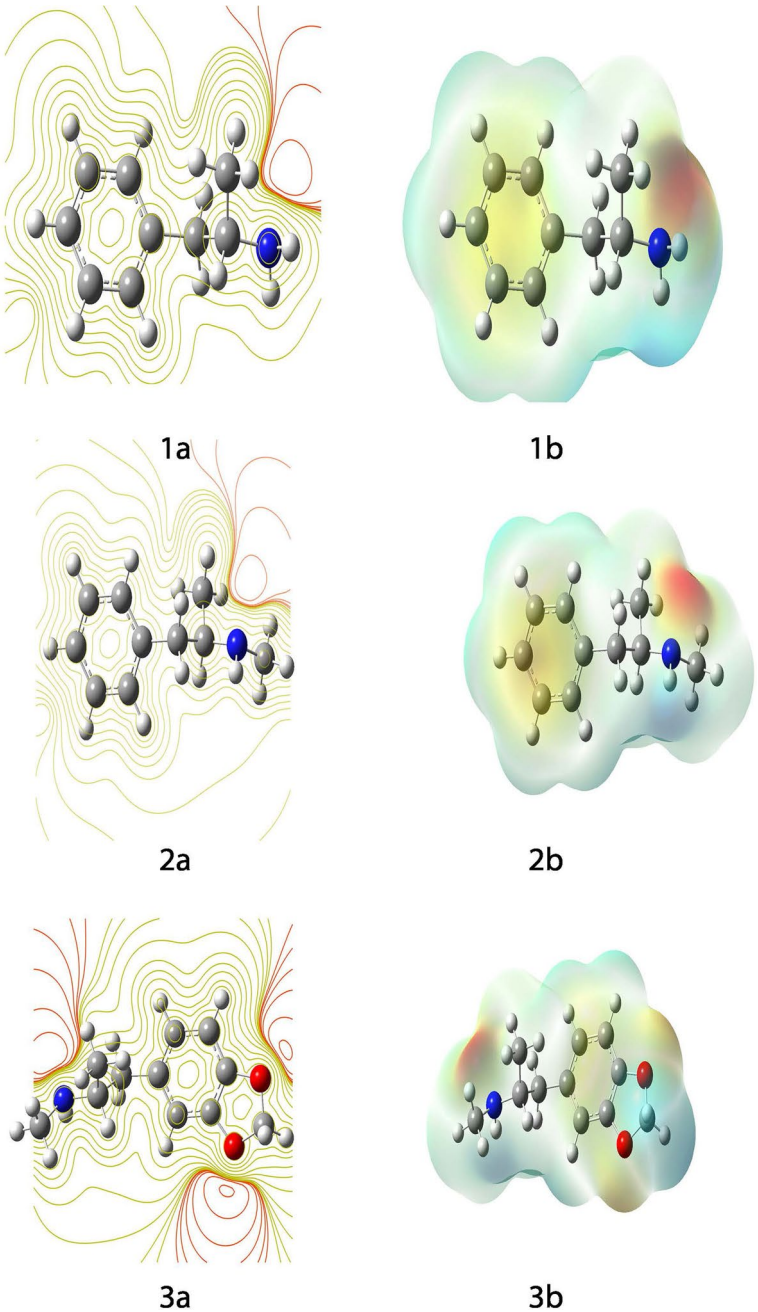

Fig. 5 Electrostatic potential map of amphetamine (1**a**, 1**b**), methamphetamine(2**a**, 2**b**) and MDMA (3**a**, 3**b**) using B3LYP/6-311+G (2d, p) in the range -4.207e-2 to +4.207e-2

molecular wave function in terms of localized electron-pair bonding units. This analysis is accomplished by transforming the given wave function into a localized form in terms of the electron densities of the molecule. In other words, NBO analysis provides a way to understand the chemical bonding and electronic structure of a molecule in terms of localized electron-pair interactions. The set of high-occupancy NBOs, each taken doubly occupied, is said to represent the "natural Lewis structure" (NLS) of the molecule [54, 55]. Delocalization effects appear as weak departures from this idealized localized

picture. According to the NBO program manual [56], energetic analysis of NBO interactions can be conducted using second-order perturbation theory in terms of the "1-electron effective Fock energy operator".

The stabilization energy associated with electron delocalization between each donor and acceptor NBO's is estimated as;

$$E^{(2)} = -n_\sigma \left[\frac{(< \sigma |F| \sigma >)^2}{\epsilon_\sigma^* - \epsilon_\sigma} \right] = -n_\sigma \left[\frac{{F_{ij}}^2}{\delta E} \right] \tag{20}$$

where F_{ij}^2 is the Fock matrix element between NBO's i and j with energies ϵ_σ and ϵ_σ^* and n_σ is the population of the donor orbital. Larger $E^{(2)}$ value indicates the strong interaction between the corresponding donor and acceptor orbitals and a greater tendency for delocalization effects. The NBO analysis of the title molecules have been done using the NBO module installed with the Guassian package. The calculated values of the stabilization energy using second order perturbation theory analysis of Fock matrix in NBO basis is shown in Tables 6, 7 and 8. The donor and acceptor orbitals having stabilization energy above 3 kcal/mol are included in the table.

Figure 6 shows the first two highly overlapping natural bonding orbitals of the three molecules plotted using Multiwfn software. The NBO plot of amphetamine shows that the donor NBO $\pi(C_1 - C_6)$ is substantially overlapped with acceptor

Table 6 Second order perturbation theory analysis of fock matrix in NBO basis: amphetamine

Sl.No	Donor NBO(i)	Acceptor NBO (j)	E(2) (Kcal/mol)	E(j)-E(i) (a.u)	F(i,j) (a.u)
1	$\sigma(C_1 - C_2)$	$\sigma^*(C_2 - C_3)$	3.20	1.26	0.057
2	$\sigma(C_1 - C_6)$	$\sigma^*(C_1 - C_2)$	3.29	1.26	0.057
3	$\sigma(C_1 - C_6)$	$\sigma^*(C_5 - C_6)$	3.13	1.26	0.056
4	$\sigma(C_2 - C_3)$	$\sigma^*(C_1 - C_2)$	3.59	1.26	0.060
5	$\sigma(C_2 - C_3)$	$\sigma^*(C_1 - C_{12})$	3.85	1.09	0.058
6	$\pi(C_2 - C_3)$	$\pi^*(C_1 - C_6)$	21.20	0.29	0.070
7	$\pi(C_2 - C_3)$	$\pi^*(C_4 - C_5)$	19.52	0.28	0.066
8	$\sigma(C_2 - H_7)$	$\sigma^*(C_1 - C_6)$	4.43	1.09	0.06
9	$\sigma(C_2 - H_7)$	$\sigma^*(C_3 - C_4)$	3.74	1.09	0.057
10	$\sigma(C_3 - H_8)$	$\sigma^*(C_1 - C_2)$	3.87	1.08	0.058
11	$\sigma(C_3 - H_8)$	$\sigma^*(C_4 - C_5)$	3.76	1.09	0.057
12	$\pi(C_4 - C_5)$	$\pi^*(C_1 - C_6)$	19.10	0.29	0.066
13	$\pi(C_4 - C_5)$	$\pi^*(C_2 - C_3)$	21.07	0.28	0.069
14	$\sigma(C_4 - H_9)$	$\sigma^*(C_2 - C_3)$	3.84	1.09	0.058
15	$\sigma(C_4 - H_9)$	$\sigma^*(C_5 - C_6)$	3.77	1.09	0.057
16	$\sigma(C_5 - C_6)$	$\sigma^*(C_1 - C_6)$	3.47	1.26	0.059
17	$\sigma(C_5 - C_6)$	$\sigma^*(C_1 - C_{12})$	3.54	1.09	0.055
18	$\sigma(C_5 - H_{10})$	$\sigma^*(C_1 - C_6)$	3.82	1.09	0.058
19	$\sigma(C_5 - H_{10})$	$\sigma^*(C_3 - C_4)$	3.76	1.09	0.057
20	$\sigma(C_6 - H_{11})$	$\sigma^*(C_4 - C_5)$	3.70	1.09	0.057
21	$\sigma(C_{12} - H_{13})$	$\sigma^*(C_1 - C_6)$	4.12	0.53	0.045
22	$\sigma(C_{12} - H_{13})$	$\sigma^*(C_{15} - C_{17})$	3.16	0.87	0.047
23	$\sigma(C_{12} - H_{14})$	$\sigma^*(C_1 - C_2)$	4.05	1.06	0.059
24	$\sigma(C_{17} - H_{18})$	$\sigma^*(C_{15} - N_{12})$	3.37	0.84	0.048
25	$LP(1)(N_{21})$	$\sigma^*(C_{15} - H_{16}))$	6.54	0.72	0.061

Table 7 Second order perturbation theory analysis of fock matrix in NBO basis: methamphetamine

Sl.No	Donor NBO(i)	Acceptor NBO (j)	E(2) (Kcal/mol)	E(j)-E(i) (a.u)	F(i,j) (a.u)
1	$\sigma(C_1 - C_6)$	$\sigma^*(C_5 - C_6)$	3.57	1.27	0.060
2.	$\sigma(C_1 - C_6)$	$\sigma^*(C_5 - C_{12})$	3.65	1.12	0.057
3.	$\pi(C_1 - C_6)$	$\pi^*(C_2 - C_3)$	19.75	0.28	0.067
4.	$\pi(C_1 - C_6)$	$\pi^*(C_4 - C_5)$	21.05	0.29	0.070
5.	$\sigma(C_1 - H_7)$	$\sigma^*(C_5 - C_6)$	3.74	1.09	0.057
6.	$\sigma(C_1 - H_7)$	$\sigma^*(C_5 - C_6)$	3.94	1.08	0.058
7.	$\pi(C_4 - C_5)$	$\pi^*(C_1 - C_6)$	20.73	0.28	0.068
8.	$\pi(C_4 - C_5)$	$\pi^*(C_2 - C_3)$	19.32	0.29	0.067
9.	$\sigma(C_2 - H_8)$	$\sigma^*(C_1 - C_6)$	3.82	1.09	0.058
10.	$\sigma(C_2 - H_8)$	$\sigma^*(C_3 - C_4)$	3.84	1.09	0.058
11	$\sigma(C_3 - C_4)$	$\sigma^*(C_4 - C_5)$	3.52	1.27	0.060
12.	$\sigma(C_3 - C_4)$	$\sigma^*(C_5 - C_12)$	3.75	1.12	0.058
13.	$\sigma(C_3 - H_9)$	$\sigma^*(C_1 - C_2)$	3.77	1.09	0.057
14.	$\sigma(C_3 - H_9)$	$\sigma^*(C_4 - C_5)$	3.92	1.09	0.058
15.	$\sigma(C_4 - C_5)$	$\sigma^*(C_3 - C_4)$	3.23	1.27	0.057
16.	$\sigma(C_4 - C_5)$	$\sigma^*(C_5 - C_6)$	3.39	1.26	0.058
17.	$\sigma(C_4 - H_{10})$	$\sigma^*(C_5 - C_6)$	4.67	1.08	0.064
18.	$\sigma(C_5 - C_6)$	$\sigma^*(C_1 - C_6)$	3.26	1.27	0.058
19.	$\sigma(C_5 - C_6)$	$\sigma^*(C_4 - C_5)$	3.33	1.26	0.058
20.	$\sigma(C_6 - H_{11})$	$\sigma^*(C_1 - C_2)$	3.80	1.09	0.057
21.	$\sigma(C_6 - H_{11})$	$\sigma^*(C_4 - C_5)$	4.60	1.09	0.063
22.	$\sigma(C_{12} - H_{13})$	$\sigma^*(C_{15} - C_{17})$	3.34	0.88	0.048
23.	$\sigma(C_{12} - H_{14})$	$\sigma^*(C_5 - C_6)$	4.29	1.06	0.060
24.	$\sigma(C_{17} - H_{20})$	$\sigma^*(C_{12} - C_{15})$	3.14	0.87	0.047
25.	$\sigma(C_{23} - H_{25})$	$\sigma^*(C_{15} - N_{21})$	3.47	0.86	0.049
26.	$LP(1)(N_{21})$	$\sigma^*(C_{15} - H_{16})$	7.83	0.67	0.065
27.	$LP(1)(N_{21})$	$\sigma^*(C_{23} - H_{26})$	7.56	0.67	0.064

NBO $\pi^*(C_4 - C_5)$ and donor NBO $\pi(C_2 - C_3)$ is substantially overlapped with acceptor NBO $\pi^*(C_1 - C_6)$, which resulted in high electron delocalization and a great tendency of charge transfer between donor and acceptor orbitals. The stabilization energy associated with electron delocalization between these orbitals are 21.41 and 21.20 Kcal/mol. For methamphetamine, the plot of NBO shows that the highest degree of overlapping is for $\pi(C_1 - C_6)$ with $\pi^*(C_4 - C_5)$ and $\pi^*(C_2 - C_3)$ and for $\pi(C_4 - C_5)$ with $\pi^*(C_2 - C_3)$ and $\pi^*(C_1 - C_6)$. The stabilization energies corresponding to these interactions are 21.05, 19.75, 19.32 and 20.73 kcal/mol respectively. These conjugate effects enhances electron delocalization and charge transfer occurs between donor and acceptor orbitals. The NBO analysis of MDMA reveals that there occurs a strong hyper conjugative interaction between $LP(2)O_{13}$ and $\pi^*(C_2 - C_3)$ and between $LP(2)O_{14}$ and $\pi^*(C_1 - C_6)$ which results in stabilization energies 25.84 and 25.5 kcal/mol. These enhanced anti bonding orbitals again conjugates with acceptor orbital $\pi^*(C_4 - C_5)$ resulting in a high stabilization energy of 216.19 and 225.23 kcal/mol. All these strong hyper conjugative interactions are confined within the ring which clearly indicates the biological activity of the molecule.

Table 8 Second order perturbation theory analysis of fock matrix in NBO basis: MDMA

Sl.No	Donor NBO(i)	Acceptor NBO (j)	E(2) (Kcal/mol)	E(j)-E(i) (a.u)	F(i,j) (a.u)
1	$\sigma(C_1 - C_2)$	$\sigma^*(C_1 - C_6)$	5.12	1.30	0.073
2.	$\sigma(C_1 - C_2)$	$\sigma^*(C_2 - C_3)$	5.17	1.30	0.073
3.	$\sigma(C_1 - C_6)$	$\sigma^*(C_1 - C_2)$	4.72	1.28	0.070
4.	$\pi(C_1 - C_6)$	$\pi^*(C_2 - C_3)$	20.35	0.29	0.070
5.	$\pi(C_1 - C_6)$	$\pi^*(C_4 - C_5)$	17.63	0.31	0.066
6.	$\sigma(C_2 - C_3)$	$\sigma^*(C_1 - C_2)$	4.75	1.28	0.070
7.	$\sigma(C_2 - C_3)$	$\sigma^*(C_3 - C_4)$	3.26	1.28	0.058
8.	$\sigma(C_2 - C_3)$	$\sigma^*(C_4 - C_15)$	3.26	1.16	0.055
9.	$\pi(C_2 - C_3)$	$\pi^*(C_4 - C_5)$	19.44	0.29	0.069
10.	$\pi(C_2 - C_3)$	$\pi^*(C_4 - C_5)$	19.26	0.31	0.070
11.	$\sigma(C_3 - C_4)$	$\sigma^*(C_2 - C_3)$	3.43	1.26	0.059
12.	$\sigma(C_3 - C_4)$	$\sigma^*(C_2 - O_13)$	6.51	1.01	0.073
13.	$\sigma(C_3 - C_4)$	$\sigma^*(C_4 - C_5)$	3.01	1.26	0.055
14.	$\sigma(C_3 - H_8)$	$\sigma^*(C_1 - C_2)$	4.04	1.08	0.059
15.	$\sigma(C_3 - H_8)$	$\sigma^*(C_4 - C_5)$	4.09	1.10	0.060
16.	$\sigma(C_4 - C_5)$	$\sigma^*(C_3 - C_4)$	3.12	1.25	0.056
17.	$\pi(C_4 - C_5)$	$\pi^*(C_1 - C_6)$	18.70	0.27	0.065
18.	$\pi(C_4 - C_5)$	$\pi^*(C_2 - C_3)$	17.25	0.27	0.063
19.	$\pi(C_4 - C_5)$	$\sigma^*(C_{15} - C_{18})$	3.16	0.63	0.043
20.	$\sigma(C_5 - C_6)$	$\sigma^*(C_1 - C_6)$	3.09	1.27	0.056
21.	$\sigma(C_5 - C_6)$	$\sigma^*(C_1 - O_{14})$	7.03	1.02	0.076
22.	$\sigma(C_5 - C_6)$	$\sigma^*(C_4 - C_5)$	3.23	1.27	0.057
23.	$\sigma(C_5 - C_6)$	$\sigma^*(C_4 - C_{15})$	3.56	1.12	0.056
24.	$\sigma(C_5 - H_9)$	$\sigma^*(C_1 - C_6)$	3.22	1.09	0.053
25.	$\sigma(C_5 - H_9)$	$\sigma^*(C_3 - C_4)$	5.02	1.06	0.065
26.	$\sigma(C_6 - H_{10})$	$\sigma^*(C_1 - C_2)$	3.97	1.08	0.059
27.	$\sigma(C_6 - H_{10})$	$\sigma^*(C_4 - C_5)$	3.49	1.10	0.055
28.	$\sigma(C_7 - O_{13})$	$\sigma^*(C_2 - C_3)$	4.82	1.40	0.074
29.	$\sigma(C_7 - O_{13})$	$\sigma^*(C_1 - C_6)$	4.77	1.40	0.073
30.	$\sigma(C_15 - H_{16})$	$\sigma^*(C_3 - C_4)$	4.27	1.04	0.060
31.	$\sigma(C_15 - H_{17})$	$\sigma^*(C_{18} - C_{20})$	3.35	0.88	0.048
32.	$\sigma(C_{20} - H_{21})$	$\sigma^*(C_{18} - N_{24})$	3.76	0.85	0.051
33.	$\sigma(C_{26} - H_{27})$	$\sigma^*(C_{18} - N_{24})$	3.47	0.86	0.049
34.	$LP(2)O_{13}$	$\pi^*(C_2 - C_3)$	25.84	0.36	0.091
35.	$LP(2)O_{13}$	$\sigma^*(C_7 - H_{11})$	6.08	0.68	0.059
36.	$LP(2)O_{13}$	$\sigma^*(C_7 - H_{12})$	3.17	0.69	0.043
37.	$LP(2)O_{14}$	$\sigma^*(C_1 - C_2)$	3.21	1.16	0.054
38.	$LP(2)O_{14}$	$\pi^*(C_1 - C_6)$	25.50	0.36	0.091
39	$LP(2)O_{14}$	$\sigma^*(C_7 - H_{11})$	6.15	0.68	0.059
40.	$LP(2)O_{14}$	$\sigma^*(C_7 - H_{12})$	3.19	0.69	0.043
41.	$LP(1)N_{24}$	$\sigma^*(C_18 - H_{19})$	7.87	0.67	0.065
42.	$LP(1)N_{24}$	$\sigma^*(C_26 - H_{28})$	7.56	0.67	0.064
43.	$\pi^*(C_1 - C_6)$	$\pi^*(C_4 - C_5)$	216.19	0.01	0.079
44.	$\pi^*(C_2 - C_3)$	$\pi^*(C_4 - C_5)$	225.23	0.01	0.081

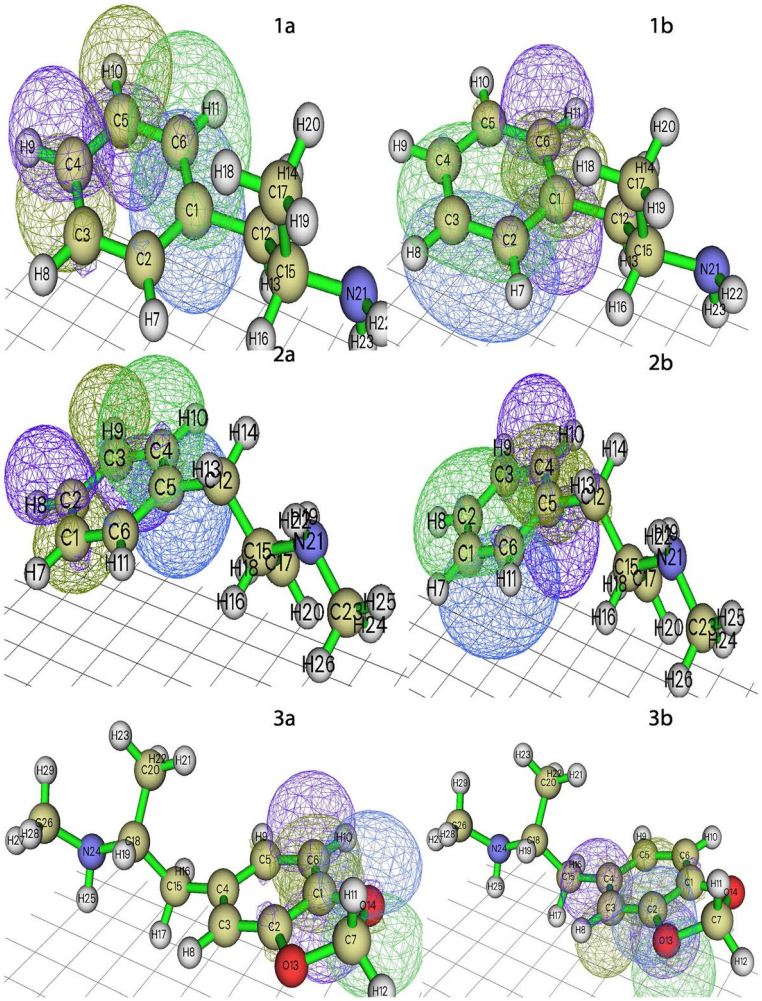

Fig. 6 Highly overlapping natural bonding orbitals (acceptor and donor) of amphetamine [1(**a**), 1(**b**)], methamphetamine [2(**a**), 2(**b**)] and MDMA [3(**a**), 3(**b**)]

Vibrational analysis

The molecular structure of these compounds does not exhibit any special symmetry, meaning that all of them belong to the C1 point group. The normal modes of vibration of these molecules belong to the 'A' irreducible representation and are both IR and Raman active. Amphetamine has a total of 63 normal modes of vibration, with 22 stretch modes, 21 bend modes, and 20 torsional modes. Methamphetamine has 72 normal modes of vibration, with 25 stretch modes, 24 bend modes, and 23 torsional modes. MDMA has 81 normal modes of vibration, with 28 stretch modes, 27 bend modes, and 26 torsional modes.

The theoretically calculated Raman activities are converted into corresponding Raman intensities using the following relation derived from the basic theory of Raman scattering [57, 58].

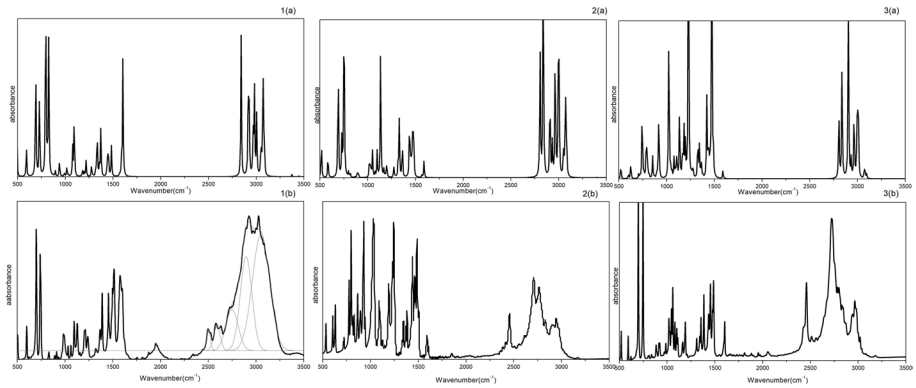

Fig. 7 The calculated and experimental IR spectra of amphetamine [1(**a**), 1(**b**)], methamphetamine [2(**a**), 2(**b**)] and MDMA [3(**a**), 3(**b**)]

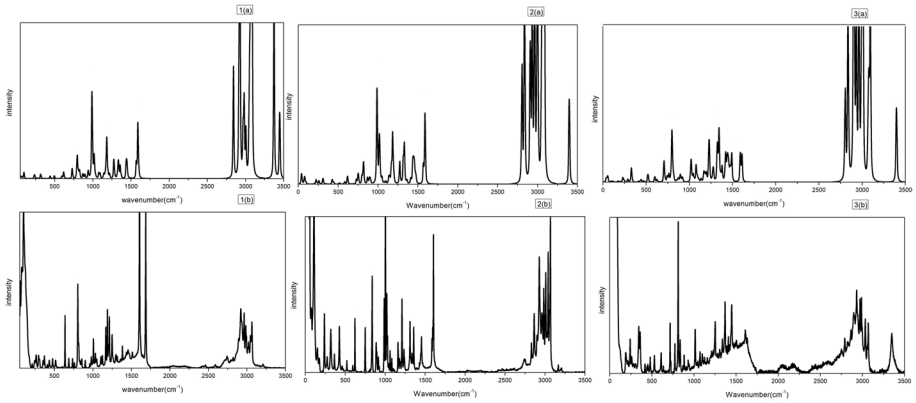

Theoretical and experimental Raman spectra of amphetamine(1(a) and 1(b)),
methamphetamine(2(a) and 2(b)) and MDMA(3(a) and 3(b))

Fig. 8 The calculated and experimental Raman spectra of amphetamine [1(**a**), 1(**b**)], methamphetamine [2(**a**), 2(**b**)] and MDMA [3(**a**), 3(**b**)]

$$l_i = \frac{f(\nu_0 - \nu_i)^4 S_i}{\nu_i \left[1 - \exp\left(\frac{-hc\nu_i}{kT}\right)\right]} \tag{21}$$

where ν_0 is the exciting frequency in cm^{-1}, ν_i is the vibrational wave number of the i^{th} normal mode and f is the common scaling factor. h, c and K are universal constants.

To improve the agreement with experimental values, the calculated wave numbers were scaled down by a factor of 0.9679 [59]. Discrepancies between the calculated and experimental wave numbers are mainly attributed to the presence of anharmonicity effects in the real system and the various approximations used in the calculation methods. The calculated and experimental IR and Raman frequencies of the title molecules are shown in the Tables 9,10 and 11 along with the PED assignments. The PED assignments are performed with VEDA 4 program [22, 23].

The experimental and calculated IR spectra of the title molecules are shown in Fig. 7 and that of Raman spectra are shown in Fig. 8.

Table 9 Experimental and theoretical vibrational wavenumbers of amphetamine with potential energy distribution

No	Experimental frequency(cm^{-1})		Calculated frequency using B3LYP/6-311+G(2d,p) (cm^{-1})		Vibrational Assignment with PED
	IR	Raman	unscaled	scaled	
1	3430.742		3561.65	3423.79	$\nu_{as}(N_{21}H_{22})(100)$
2	3345.89		3484.88	3349.99	$\nu_{s}(N_{21}H_{23})(100)$
3	3085.547	3066.34	3185.59	3062.29	$\nu_{s}(C_5H_{10})(84)$
4			3174.02	3051.15	$\nu_{s}(C_2H_7)(87)$
5		3047.02	3165.79	3043.25	$\nu_{s}(C_6H_{11})(87)$
6	3025.764	3028.26	3155.68	3033.53	$\nu_{s}(C_3H_8)(87)$
7	2998.766	3021.83	3149.65	3027.74	$\nu_{s}(C_4H_9)(78)$
8	2975.624	2985.68	3104.19	2984.01	$\nu_{s}(C_{12}H_{13})(77)+\nu_{as}(C_{17}H_{20})(18)$
9	2965.982	2964.94	3079.55	2960.35	$\nu_{s}(C_{17}H_{19})(92)$
10		2932.43	3064.98	2946.31	$\nu_{as}(C_{12}H_{14})(83)+\nu_{as}(C_{17}H_{18})(15)$
11	2925.484	2920.69	3023.34	2906.30	$\nu_{s}(C_{12}H_{13})(18)+\nu_{s}(C_{17}H_{20})(80)$
12	2894.629	2895.84	3012.48	2895.88	$\nu_{as}(C_{12}H_{14})(15)+\nu_{s}(C_{17}H_{18})(84)$
13		2869.6	2936.07	2822.38	$\nu_{s}(C_{15}H_{16})(97)$
14	1598.699	1606.18	1656.77	1592.63	$\beta(H_{23}N_{21}H_{22})(76)+\tau(H_{22}N_{21}C_{15}C_{12})(22)$
15	1575.557	1576.91	1642.82	1579.23	$\nu_{s}(C_5C_4)(57)+\beta(H_9C_4C_5)(20)$
16	1511.918	1563.01	1621.23	1558.48	$\nu_{as}(C_6C_5)(61)+\beta(H_7C_2C_3)(10)$
17	1498.419	1469.74	1532.36	1473.04	$\beta(H_{11}C_6C_5)(50)+\beta(C_6C_5C_4)(13)$
18	1454.064	1454.09	1501.02	1442.88	$\beta(H_{18}C_{17}H_{20})(62)+\tau(H_{20}C_{17}C_{15}C_{12})(17)$
19		1441.55	1495.57	1437.72	$\beta(H_{14}C_{12}C_{13})(65)+\gamma(C_{15}C_{17}C_{12}C_{16})(10)$
20		1435.27	1489.76	1432.06	$\beta(H_{19}C_{17}H_{18})(51)$
21	1390.423	1427.41	1484.29	1426.90	$\beta(H_9C_4C_5)(48)$
22	1367.283	1383.29	1418.24	1363.31	$\beta(H_{16}C_{15}C_{17})(60)$
23	1332.571	1337.34	1402.44	1347.78	$\beta(H_{20}C_{17}H_{19})(76)$
24	1321	1316.66	1378.53	1325.10	$\gamma(H_{18}C_{17}C_{15}C_{12})(62)$
25		1300.72	1363.98	1311.26	$\beta(H_8C_3C_4)[12]+\beta(H_{10}C_5C_4)[50]$
26	1297.858	1295.93	1333.74	1282.11	$\nu_{as}(C_2C_3)(62)$
27	1238.076	1249.5	1318.24	1267.21	$\tau(H_{14}C_{12}C_1C_6)(50)$
28	1211.077	1214.1	1258.88	1210.27	$\beta(H_{22}N_{21}H_{22})(39)$
29	1203.363	1188.26	1238.23	1190.26	$\beta(H_{13}C_{12}C_1)(10)+\tau(H_{18}C_{17}C_{15}C_{12})(18)$
30	1180.22	1167.2	1220.31	1173.06	$\nu_{s}(C_4C_3)(44)+\beta(H_{11}C_6C_5)[12]+\beta(C_5C_4C_3)(12)$
31	1157.08		1204.63	1158.01	$\nu_{s}(C_5C_4)(20)+\beta(H_9C_4C_5)[64]$
32	1128.153	1124.94	1182.50	1136.73	$\beta(H_7C_2C_3)(62)$
33	1095.369	1105.35	1130.32	1086.61	$\nu_{s}(N_{21}C_{15})(22)+\beta(H_{13}C_{12}C_1)[15]$
34	1060.657	1049.63	1113.08	1070.07	$\nu_{s}(N_{21}C_{15})(15)+\beta(H_{10}C_5C_4)(13)+\tau(H_{20}C_{17}C_{15}C_{12})(12)+\gamma(N_{21}C_{12}C_{17}C_{15})(10)$
35	1031.73	1031.52	1068.59	1027.19	$\nu_{s}(C_{12}C_1)(17)+\beta(H_{13}C_{12}C_1)(18)$
36	991.2319	1006.77	1051.07	1010.39	$\nu_{s}(C_1C_6)(27)+\beta(H_{11}C_6C_5)[20]+\beta(C_6C_5C_4)(31)$
37			1024.92	985.10	$\nu_{s}(C_{17}C_{15})(39)+\beta(H_{22}N_{21}C_{15})(25)$
38	983.5181		1020.55	981.02	$\nu_{as}(C_1C_6)(39)+\beta(C_6C_5C_4)(25)$
39		978.625	996.46	957.90	$\tau(H_8C_3C_4C_5)(60)+\tau(C_2C_3C_4C_5)(24)$
40		960.366	976.93	939.12	$\tau(H_9C_4C_3C_2)(79)$
41	912.1648	900.329	970.90	933.44	$\nu_{s}(C_{17}C_{15})(12)+\nu_{s}(N_{21}C_{15})[26]+\tau(H_{22}N_{21}C_{15}C_{12})(10)+\tau(H_{20}C_{17}C_{15}C_{12})(11)$
42	892.88		925.22	889.44	$\tau(H_{11}C_6C_1C_{12})(77)$
43		855.023	899.66	864.78	$\tau(H_{13}C_{12}C_1C_6)(46)$

Table 9 (continued)

No	Experimental frequency(cm^{-1})		Calculated frequency using B3LYP/6-311+G(2d,p) (cm^{-1})		Vibrational Assignment with PED
	IR	Raman	unscaled	scaled	
44	831.1692	828.063	854.81	821.60	$\tau(H_{22}N_{21}C_{15}C_{12})(12)+\tau(H_{10}C_5C_4C_3)(46)$
45		816.24	853.96	820.48	$\tau(H_{22}N_{21}C_{15}C_{12})(12)+\tau(H_{10}C_5C_4C_3)(47)$
46		804.402	839.71	807.19	$\nu_s(C_{15}C_{12})(45)$
47		760.287	821.53	789.73	$\tau(H_{22}N_{21}C_{15}C_{12})(25)$
48	738.6028	736.439	754.08	724.89	$\tau(H_7C_2C_3C_4)(20)+\tau(H_8C_3C_4C_5)(11)+\tau(C_6C_5C_4C_3)(33)$
49	698.105	688.545	713.38	685.73	$\tau(H_7C_2C_3C_4)(61)+\tau(C_6C_5C_4C_3)(15)$
50		638.659	638.62	613.90	$\beta(C_1C_6C_5)(82)$
51	597.8241		612.84	589.11	$\beta(C_2C_3C_4)(46)+\tau(N_{21}C_{12}C_{17}C_{15})(23)$
52	503.3298	476.727	511.35	491.53	$\tau(H_8C_3C_4C_5)(12)+\tau(C_2C_3C_4C_5)(14)+\tau(C_{12}C_6C_2C_1)(28)$
53	455.1182	434.447	453.61	436.17	$\beta(C_{12}C_{15}C_{17})(36)+\tau(N_{21}C_{12}C_{17}C_{15})(23)$
54			415.87	399.77	$\tau(C_1C_6C_5C_4)(83)$
55		370.645	391.38	376.21	$\beta(C_{17}C_{15}C_{12})(46)$
56		352.841	353.19	339.55	$\beta(C_{12}C_1C_2)$[56]
57		295.625	326.99	314.30	$\beta(C_{12}C_{15}C_{17})(30)$
58		263.278	278.28	267.67	$\tau(H_{23}N_{21}C_{15}C_{12})(66)+\tau(H_{19}C_{17}C_{15}C_{12})(19)$
59		245.257	243.25	234.18	$\beta(C_{15}C_{12}C_1)(29)+\tau(C_2C_3C_4C_5)$[19]$+\tau(C_6C_5C_4C_{13})(16)$
60		210.916	235.46	226.55	$\tau(H_{23}N_{21}C_{15}C_{12})(20)+\tau(H_{19}C_{17}C_{15}C_{12})(50)$
61		99.7619	100.48	96.60	$\beta(C_{15}C_{12}C_1)(33)+\tau(C_{12}C_6C_2C_1)(34)$
62		77.7342	70.29	67.66	$\tau(C_{17}C_{15}C_{12}C_1)(71)$
63		57.4942	43.34	41.67	$\tau(C_{15}C_{12}C_1C_6)(80)$

Assignment of spectra

4000-2800 cm^{-1}

The vibrational wave numbers expected to appear in this region are those correspond to the C-H stretch modes of CH_2, CH_3, and aromatic groups, as well as the N-H stretch mode. For the three molecules, the C-H stretch belonging to CH_3 and CH_2 group vibrations is typically found between 2800-3020 cm^{-1} [60, 61]. In the vibrational spectrum of amphetamine, the CH stretch band at 2804 cm^{-1} belonging to the CH_3 group is absent. The aromatic C-H vibrations of all three molecules are observed and calculated between 2900-3090 cm^{-1} (as shown in Table 9). Both the asymmetric and symmetric N-H stretch bands of amphetamine appear near 3430 and 3345 cm^{-1} in both the experimental and calculated spectra. For methamphetamine, the N-H band is at 3535 cm^{-1}, and for MDMA, it is at 3390 cm^{-1}, which are pure bands [62, 63].

1700-1000 cm^{-1}

The ring vibrations, C-H and N-H in-plane and out-plane bending vibrations and N-C stretching vibrations are expected in this region. The ring modes were observed and calculated for amphetamine between 1576-1158 cm^{-1} and for methamphetamine, the vibrational wave numbers corresponding to the C-C stretch are found between 1271-1602 cm^{-1} both in theoretical and experimental spectra. For MDMA, four ring modes are observed and calculated between the range 1211- 1608 cm^{-1} as shown in Table 9. The C-H bending vibrations of the three molecules are identified between 1128-1498/

Table 10 Experimental and theoretical vibrational wave numbers of methamphetamine with potential energy distribution

No	Experimental frequency(cm^{-1})		Calculated frequency using B3LYP/6-311+G(2d, p)(cm^{-1})		Vibrational Assignment with PED
	IR	Raman	unscaled	scaled	
1	3535.03		3510.79	3398	$\nu_s(N_{21}H_{22})(100)$
2	3103.03	3167.26	3185.64	3082.34	$\nu_s(C_4H_{10})(92)$
3	3081.82		3173.34	3071.48	$\nu_s(C_2H_8)(12)+\nu_s(C_6H_{11})(83)$
4	3064.46	3067.63	3165.76	3064.14	$\nu_s(C_1H_7)(86)$
5		3056.04	3154.77	3053.5	$\nu_s(C_3H_9)(88)$
6	3039.39		3149.82	3048.71	$\nu_{as}(C_2H_8)(79)+\nu_s(C_6H_{11})(14)$
7	3020.11	3008.94	3104.35	3004.7	$\nu_{as}(C_{17}H_{18})(87)+\nu_{as}(C_{23}H_{24})(12)$
8		3088.94	3099.13	2999.64	$\nu_s(C_1H_7)(86)$
9	2979.61		3093.26	2993.96	$\nu_{as}(C_{17}H_{18})(11)+\nu_s(C_{23}H_{24})(82)$
10	2966.11	2984.38	3062.34	2964.04	$\nu_{as}(C_{12}H_{14})(70)+\nu_{as}(C_{17}H_{19})(12)+\nu_s(C_{15}H_{16})(16)$
11		2961.05	3061.54	2963.24	$\nu_{as}(C_{12}H_{14})(15)+\nu_s(C_{15}H_{16})(78)$
12	2944.89	2928.32	3031.16	2933.86	$\nu_{as}(C_{12}H_{13})(86)$
13	2896.68	2899.77	3005.11	2908.64	$\nu_s(C_{12}H_{14})(14)+\nu_s(C_{17}H_{19})(86)$
14	2831.11	2830.06	2931.95	2837.83	$\nu_s(C_{23}H_{26})(96)$
15	2798.32	2807.56	2898.1	2805.07	$\nu_s(C_{23}H_{25})(97)$
16	1602.62	1598.87	1643.06	1590.31	$\nu_s(C_2C_1)(56)+\gamma(H_8C_2C_3)(14)$
17	1556.34	1584.62	1621.17	1569.13	$\nu_s(C_5C_4)(60)+\gamma(C_2C_1C_6)(12)$
18	1486.61		1531.81	1482.64	$\gamma(C_5C_4C_3)(19)+\beta(H_7C_1C_2)(55)$
19	1475.34	1469.74	1522.15	1473.29	$\gamma(H_{22}N_{21}C_{23})(16)+\beta(H_{24}C_{23}H_{26}C_{16})(50)+\tau(H_{24}C_{23}N_{21}C_{15})(15)$
20			1508.22	1459.80	$\gamma(H_{18}C_{17}H_{20})(68)+\tau(H_{13}C_{12}C_5C_6)(21)$
21		1454.09	1505.29	1456.97	$\beta(H_{22}N_{21}C_{23})(23)+\beta(H_{19}C_{17}H_{18})(41)$
22			1494.61	1446.63	$\beta(H_{14}C_{12}H_{13})(57)$
23			1488.92	1441.13	$\gamma(H_{25}C_{23}H_{24})(70)+\tau(H_{20}C_{17}C_{15}C_{12})(11)$
24			1486	1438.29	$\nu_{as}(C_1C_6)(12)+\beta(H_{11}C_6C_5)(50)$
25	1434.84	1427.41	1483.64	1436.01	$\gamma(H_{22}N_{21}C_{23})[114]+\beta(H_{14}C_{12}H_{13})(17)+\beta(H_{19}C_{17}H_{18})[32]$
26	1384.7		1457.96	1411.16	$\beta(H_{26}C_{23}H_{25})(84)$
27	1355.77	1356.39	1407.71	1362.52	$\beta(H_{20}C_{17}H_{19})(90)$
28	1342.27	1334.17	1376.74	1332.55	$\beta(H_{10}C_4C_5)(13)+\beta(H_{13}C_2C_5)(27)+\tau_o(H_{16}C_{15}N_{21}C_{23})(13)$
29			1373.19	1329.11	$\beta(H_{10}C_4C_5)(13)+\gamma(H_{13}C_{12}C_5)(25)+\tau_o(H_{18}C_{17}C_{15}C_{12})(24)$
30	1309.48	1310.29	1360.55	1316.87	$\beta(H_{10}C_4C_5)[44]+\tau_o(H_{16}C_{15}N_{21}C_{23})(22)$
31	1270.91	1233.42	1333.40	1290.59	$\nu_s(C_3C_2)(66)+\beta(H_9C_3C_4)[11]$
32	1257.41	1210.87	1314.84	1272.63	$\gamma(H_{13}C_{12}C_{15})(19)+\tau_o(H_{18}C_{17}C_{15}C_{12})(14)+\gamma(H_{16}C_{15}C_{17})[10]$
33	1209.2	1189.87	1239.89	1199.6	$\nu_{as}(C_{12}C_5)(10)+\gamma(H_{16}C_{15}C_{17})[16]+\tau_o(H_{19}C_{17}C_{15}C_{12})(14)$
34	1189.91	1180.17	1223.85	1184.56	$\nu_s(C_{12}C_5)(44)+\beta(C_4C_3C_2)(14)$
35	1164.84	1160.71	1207.73	1168.96	$\beta(H_{24}C_{23}H_{26})(11)+\tau(H_{24}C_{23}N_{21}C_{15})(32)$
36			1204.79	1166.12	$\nu_s(C_2C_1)(26)+\beta(H_8C_2C_3)[61]$
37	1112.77		1182.46	1144.49	$\gamma(H_9C_3C_4)(74)$
38	1101.20		1172.95	1135.29	$\nu_{as}(N_{21}C_{23})(41)+\tau(H_{20}C_{17}C_{15}C_{12})(13)$
39	1081.92	1082.45	1135.20	1098.76	$\nu_{as}(N_{21}C_{23})(10)+\beta(H_{16}C_{15}C_{17})(10)+\tau_O(H_{20}C_{17}C_{15}C_{12})(31)$
40	1058.77	1061.13	1113.46	1077.71	$\gamma(H_{11}C_6C_5)(11)+\tau(H_{20}C_{17}C_{15}C_{12})(14)$
41	1045.27	1044.7	1084.92	1050.09	$\nu_{as}(N_{21}C_{15})(20)+\nu_s(C_{17}C_{15})[17]+\tau(H_{14}C_{12}C_5C_6)(17)$
42	1027.92		1066.2	1031.97	$\nu_s(C_1C_6)(11)+\beta(H_{16}C_{15}C_{17})(21)+\tau_o(H_{13}C_{12}C_5C_6)(11)$
43	1020.20	1029.88	1054.61	1020.75	$\nu_{as}(N_{21}C_{15})(17)+\nu_{as}(C_{17}C_{15})(17)+\tau_o(H_{13}C_{12}C_5C_6)(11)+\tau_o(H_{24}C_{23}N_{21}C_{15})(15)$

Table 10 (continued)

No	Experimental frequency(cm^{-1})		Calculated frequency using B3LYP/6-311+G(2d, p)(cm^{-1})		Vibrational Assignment with PED
	IR	Raman	unscaled	scaled	
44		1019.98	1050.43	1016.71	$\nu_s(C_4C_3)(29)+\gamma(C_5C_4C_3)(25)\gamma(H_7C_1C_2)(26)$
45	987.42	986.91	1021.34	988.56	$\nu_s(C_4C_3)(49)+\beta(C_5C_4C_3)(37)$
46	970.06		997.05	965.04	$\tau(H_9C_3C_4C_5)(80)$
47	923.77		977.17	945.8	$\tau_o(H_8C_2C_3C_4)(82)$
48	914.13	915.38	935.73	905.69	$\nu_s(N_{21}C_{15})(11)+\tau(H_{11}C_6C_5C_{12})(33)+\tau_o(H_{14}C_{12}C_5C_6)(10)$
49	885.2	895.31	922.39	892.78	$\nu_s(C_{17}C_{15})(14)+\tau(H_{11}C_6C_5C_{12})(43)+\tau(H_{14}C_{12}C_5C_6)(11)$
50	852.42	886.93	898.57	869.72	$\tau_o(H_{13}C_{12}C_5C_6)(15)+\tau(H_{19}C_{17}C_{15}C_{12})(33)$
51	836.99	836.5	854.11	826.69	$\tau(H_7C_1C_2C_3)(96)$
52	809.99		844.23	817.13	$\nu_s(C_{15}C_{12})(32)$
53	802.28		825.82	799.31	$\nu_s(C_1C_6)(12)+\nu_{as}(C_{15}C_{12})(20)+\gamma(C_4C_3C_2)(15)$
54	748.28	750.08	777.29	752.34	$\gamma(H_{22}N_{21}C_{23})(12)+\tau(H_{22}N_{21}C_{15}C_{12})(41)$
55	700.06		753.54	729.35	$\tau_o(H_{22}N_{21}C_{15}C_{12})(13)+\tau(H_{10}C_4C_5C_{12})(43)$
56			713.56	690.66	$\tau(H_{10}C_4C_5C_{12})(31)+\tau_o(C_4C_3C_2C_1)(47)$
57	620.99	621.39	638.56	618.06	$\beta(C_2C_1C_6)(80)$
58	592.06	593.69	603.48	584.11	$\beta(C_{23}N_{21}C_{15})(60)$
59	518.78	520.55	532.51	515.41	$\beta(C_3C_2C_1)(29)+\tau_O(C_{12}C_6C_4C_5)(27)$
60	462.85		458.85	444.12	$\tau_O(C_{17}C_{12}N_{21}C_{15})(31)$
61	428.14	427.38	439.61	425.49	$\gamma(C_3C_2C_1)(22)+\tau_O(C_{17}C_{12}N_{21}C_{15})(10)+\tau_O(C_{12}C_6C_4C_5)(26)$
62	406.92		415.55	402.21	$\tau_o(H_8C_3C_2C_4)(11)+\tau(C_3C_2C_1C_6)(83)$
63		365.31	362.52	350.88	$\gamma(N_{21}C_{15}C_{12})(58)+\tau_o(H_{19}C_{17}C_{15}C_{12})(14)$
64		318.91	321.11	310.80	$\beta(C_{12}C_5C_4)(50)+\tau(H_{25}C_{23}N_{21}C_{15})(10)$
65		274.07	269.15	260.51	$\beta(C_{17}C_{15}N_{21})(43)$
66		239.84	246.27	238.36	$\gamma(C_{12}C_5C_4)(12)+\tau(H_{25}C_{23}N_{21}C_{15})(61)$
67			231.87	224.43	$\beta(C_{15}C_{12}C_5)(48)+\tau_o(N_{21}C_{15}C_{12}C_5)(14)$
68		176.44	211.21	204.43	$\tau_o(H_{26}C_{23}N_{21}C_{15})(87)$
69		108.926	100.11	96.89	$\tau(H_{25}C_{23}N_{21}C_{15})(11)+\tau(C_5C_4C_3C_2)(47)+\tau(N_{21}C_{15}C_{12}C_5)(14)$
70		77.73	82.62	79.97	$\beta(C_{15}C_{12}C_5)(16)+\tau(C_5C_4C_3C_2)(16)+\tau(N_{21}C_{15}C_{12}C_5)(39)$
71		53.81	54.28	52.54	$\tau(C_{23}N_{21}C_{15}C_{12})(71)$
72			42.41	41.05	$\tau(C_{15}C_{12}C_5C_6)(78)$

1124-1469 cm^{-1} for IR/Raman and 1136-1473 cm^{-1} in the theoretical spectrum [61, 64]. The C-H bending vibration observed at 1411 cm^{-1} due to the CH_3 group for methamphetamine and MDMA are absent in the corresponding amphetamine IR spectra. The strong peak appears at 1598/1606 cm^{-1} in the experimental IR/Raman spectra of amphetamine is assigned to H-N-H in plane bending mode while the same is absent in the spectra of methamphetamine and MDMA. The week band at 1086 cm^{-1} in the calculated spectra of amphetamine is assigned to N-C stretching mode which is at 1095 cm^{-1}/1105 cm^{-1} for IR/Raman experimental spectra. The N-C stretching vibration appears at 1101/1097 cm^{-1} in the IR spectra of methamphetamine/amphetamine [65].Some additional peaks are found in the spectra of MDMA near 1000 cm^{-1} which is due to the stretch and bend modes of O-C. The peak appears at 1388/1379 cm^{-1} in the experimental/calculated IR spectrum of MDMA is assigned to the torsional mode

Table 11 Experimental and theoretical vibrational wave numbers of MDMA with potential energy distribution

No	Experimental frequency(cm^{-1})		Calculated frequency using B3LYP/6-311+G(2d, p)(cm^{-1})		Vibrational Assignment with PED
	IR	Raman	unscaled	scaled	
1	3389.71		3510.76	3398.07	$\nu_s(N_{24}H_{25})(100)$
2		3067.63	3198.39	3095.72	$\nu_s(C_5H_9)(87)$
3	3068.91	3056.04	3183.98	3081.12	$\nu_s(C_3H_8)(92)$
4	3057.33	3039.83	3172.58	3070.74	$\nu_s(C_6H_{10})(92)$
5	3033.41	3021.83	3110.04	3010.21	$\nu_s(C_7H_{11})(94)$
6	2997.32		3102.72	3003.12	$\nu_{as}(C_{20}H_{23})(91)$
7	2988.27		3098.29	2998.83	$\nu_{as}(C_{20}H_{21})(95)$
8		2984.38	3091.99	2992.73	$\nu_{as}(C_{26}H_{27})(89)$
9	2971.43		3063.96	2965.61	$\nu_{as}(C_{15}H_{17})(85)+\nu_s(C_{20}H_{22})(13)$
10	2931.12	2961.05	3060.91	2962.65	$\nu_s(C_{18}H_{19})(93)$
11	2899.77	2928.52	3030.28	2933.00	$\nu_{as}(C_{15}H_{16})(93)$
12	2897.15		3001.68	2905.32	$\nu_s(C_{15}H_{17})(13)+\nu_s(C_{20}H_{22})(85)$
13		2899.77	2999.14	2902.87	$\nu_s(C_7H_{12})(14)$
14	2836.66	2864.34	2931.28	2837.18	$\nu_s(C_{26}H_{28})(96)$
15	2804.91	2830.06	2897.38	2804.37	$\nu_s(C_{26}H_{29})(99)$
16	1607.72	1604.64	1662.37	1609.01	$\nu_{as}(C_1C_6)(66)$
17	1590.79	1593.87	1643.08	1590.34	$\nu_s(C_3C_2)(61)+\beta(H_8C_3C_4)(10)$
18	1488.48		1539.80	1490.36	$\beta(H_{12}C_7H_{11})(84)$
19	1480.67		1524.07	1475.14	$\gamma(H_{25}N_{24}C_{26})(10)+\gamma(H_9C_5C_6)(25)$
20	1472.86		1521.29	1472.45	$\beta(H_{18}C_{17}H_{20})(68)+\gamma(H_9C_5C_6)(11)+\gamma(H_{27}C_{26}H_{29})(12)$ $+\gamma(H_{29}C_{26}H_{28})(21)$
21			1507.36	1458.97	$\gamma(H_{17}C_{15}H_{16})(69)$
22	1465.04	1454.09	1505.33	1457.01	$\beta(H_{25}N_{24}C_{26})(19)+\beta(H_{29}C_{26}H_{28})(40)+\tau_o(H_{23}C_{20}C_{18}C_{15})(11)$
23	1447.82		1493.56	1445.61	$\beta(H_{21}C_{20}H_{23})(57)$
24			1488.94	1441.14	$\beta(H_{22}C_{20}H_{21})(71)+\tau(H_{23}C_{20}C_{18}C_{15})(10)$
25			1483.45	1435.83	$\beta(H_{25}N_{24}C_{26})[13]+\beta(H_{27}C_{26}H_{29})(51)$
26	1421.12		1468.44	1421.29	$\nu_s(C_6C_5)(24)+\gamma(C_4C_5C_6)[16]+\gamma(H_{10}C_6C_5)(19)$
27	1406.96		1458.56	1411.73	$\beta(H_{28}C_{26}H_{27})(90)$
28	1388.03		1425.33	1379.57	$\tau_o(H_{11}C_7O_{13}C_2)(75)$
29	1367.48	1356.39	1408.17	1362.97	$\beta(H_{23}C_{20}H_{22})(83)$
30	1346.87		1388.61	1344.03	$\nu(O_{14}C_1)[57]+\beta(H_{19}C_{18}C_{20})(14)$
31	1335.75	1334.17	1374.60	1330.47	$\beta(H_{16}C_{15}C_4)[48]+\tau_o(H_{17}C_{15}C_4C_3)(10)$
32	1318.26	1310.29	1368.23	1324.30	$\nu_as(O_{14}C_1)(10)+\tau_o(H_{19}C_{18}N_{24}C_{26})(36)+\beta(H_{16}C_{15}C_4)[13]$
33	1275.15		1319.56	1277.20	$\gamma(H_{16}C_{15}C_4)[17]+\tau_o(H_{17}C_{15}C_4C_3)(37)$
34	1214.1	1233.42	1304.81	1262.92	$\beta(H_8C_3C_4)[58]+\tau(H_{17}C_{15}C_4C_3)(12)$
35	1207.64	1210.87	1269.54	1228.78	$\nu_s(C_4C_5)(58)$
36	1197.96		1236.51	1196.82	$\beta(H_{19}C_{18}C_{15})(26)+\tau(H_{21}C_{20}C_{18}C_{15})[14]$
37	1181.78		1221.06	1181.86	$\nu_s(O_{13}C_{12})(11)+\gamma(C_1C_6C_5)(11)+\gamma(H_{11}C_7O_{13})(37)$ $+\tau_o(H_{12}C_7O_{13}C_2)(10)$
38	1170.44	1160.71	1208.63	1169.83	$\tau_o(H_{28}C_{26}N_{24}C_{18})(26)$
39	1159.09		1204.53	1165.86	$\nu_{as}(O_{13}C_2)(12)+\gamma(H_9C_5C_6)(13)+\gamma(H_{11}C_7O_{13})(26)$ $+\tau_o(H_{12}C_7O_{13}C_2)(12)$
40	1139.96		1173.64	1135.96	$\nu_s(N_{24}C_{26})(41)+\tau(H_{23}C_{20}C_{18}C_{15})(38)$
41	1115.15		1146.16	1109.36	$\nu_s(C_4C_5)(10)+\nu_s(C_6C_5)[14]+\beta(H_{10}C_6C_5)(44)$
42	1103.72		1142.17	1105.50	$\beta(H_{11}C_7O_{13})(20)+\tau(H_{12}C_7O_{13}C_2)(38)+\tau_o(C_{17}O_{14}C_1C_2)(14)$

Table 11 (continued)

No	Experimental frequency(cm^{-1})		Calculated frequency using B3LYP/6-311+G(2d, p)(cm^{-1})		Vibrational Assignment with PED
	IR	Raman	unscaled	scaled	
43	1097.18		1130.44	1094.14	$\nu_s(N_{24}C_{26})(16) + \tau(H_{23}C_{20}C_{18}C_{15})(38)$
44	1079.18	1061.13	1114.36	1078.58	$\nu_s(C_2C_1)(35)$
45	1070.98		1089.69	1054.71	$\nu_{as}(N_{24}C_{18})(17)+\nu_{as}(C_{20}C_{18})(11)+\beta(H_{19}C_{18}C_{20})(11)$ $+\tau_o(H_{21}C_{20}C_{18}C_{15})(19)$
46	1046.34		1076.73	1042.17	$\nu_s(C_{18}C_{15})(13)+\beta(H_{19}C_{18}C_{20})(14)+\tau_o(H_{22}C_{20}C_{18}C_{15})(11)$
47	1033.17	1029.88	1058.03	1024.08	$\nu_s(O_{14}C_7)(28)+\gamma(O_{14}C_1C_6)(26)$
48	1015.03	1019.98	1053.32	1019.50	$\nu_s(N_{24}C_{18})(13)+\nu_as(C_{18}C_5)(11)$
49	942.07	986.91	953.30	922.69	$\nu_s(C_2C_1)(15)+\nu_as(O_{14}C_7)(24)+\gamma(O_{14})C_1C_6)(10)$
50	930.4		946.61	916.23	$\nu_as(O_{14}C_7)(18)+\gamma(C_{17})O_{14}C_1)(32)$
51			936.16	906.11	$\tau(H_{10}C_6C_5C_4)(60)+\tau(C_2C_1C_6C_5)(15)$
52		895.31	923.86	894.20	$\nu_{as}(N_{24}C_{12})(32)+\nu_as(C_{20}C_{18})(22)+\tau(H_{21})C_{20}C_{18}C_{15})(17)$
53	883.58	886.93	900.67	871.76	$\tau(H_{29}C_{26}N_{24}C_{18})(22)+\tau_o(H_{19}C_{18}N_{24}C_{18})(13)$
54	834.81	836.5	882.02	853.70	$\tau(H_8C_3C_4C_{15})(67)$
55	811.17		843.39	816.31	$\nu_s(C_{18}C_{15})(26)+\tau_o(H_9C_5C_6C_1)(28)$
56			826.42	799.89	$\nu_s(C_{15}C_4)(66)$
57			813.80	787.67	$\nu_s(C_{18}C_{15})(17)+\tau(H_9C_5C_6C_1)(48)$
58	772.19	750.08	789.24	763.90	$\nu_s(O_{13}C_2)(19)+\beta(C_1C_6C_5)(17)+\tau(H_{25}N_{24}C_{18}C_{15})(14)$
59			769.38	744.67	$\nu_{as}(O_{13}C_2)(10)+\nu_s(N_{24}C_{18})(12)+\gamma(H_{25}N_{24}C_{26})(10)$ $+\tau_O(H_{25}N_{24}C_{18}C_{15})(39)$
60	722.78		744.18	720.29	$\tau_O(H_{10}C_6C_5C_4)(13)+\tau_O(C_4C_5C_6C_1)(64)$
61	715.95		731.01	707.55	$\beta(C_3C_2C_1)(64)$
62	609.28	621.39	646.06	625.32	$\gamma(O_{13}C_2C_1)(19)+\tau_o(C_3C_2C_1C_6)(28)$
63			619.55	599.67	$\gamma(O_{13}C_2C_1)(33)+\tau(C_3C_2C_1C_6)(18)$
64	529.29		538.38	521.1	$\nu_s(O_{13}C_2)(66)+\beta(C_4C_5C_6)(19)+\gamma(C_1C_6C_5)(10)$
65	478.49		485.02	469.45	$\beta(N_{24}C_{18}C_{15})(40)$
66	452.09		457.46	442.78	$\beta(N_{12}C_{18}C_{15})(10)+\tau_o(H_{16}C_{15}C_4C_3)(19)+\tau(C_{20}C_{15}N_{24}C_{18})(35)$
67		427.38	444.38	430.113	$\beta(C_{15}C_4C_5)(63)$
68	416.77		425.64	411.98	$\tau(C_2C_1C_6C_5)(49)+\tau(O_{13}C_3C_2C_1)(12)$
69	343.92		341.51	330.54	$\tau(O_{13}C_3C_2C_1)(49)$
70	304.59	318.912	338.67	327.79	$\beta(C_{20}C_{18}N_{24})(58)+\tau(C_{20}C_{15}N_{24}C_{18})(10)$
71	279.47		297.79	288.23	$\beta(C_2C_1C_6)(38)+\tau(H_{27}C_{26}N_{24}C_{18})(19)$
72	259.68	239.84	253.81	245.66	$\beta(C_{26}N_{24}C_{18})(26)+\tau_o(H_{27}C_{26}N_{24}C_{18})(19)$
73	239.843		239.17	231.49	$\gamma(C_{26}N_{24}C_{18})(15)+\tau_o(O_{13}C_2C_6C_1)(59)$
74			235.89	228.32	$\beta(C_{26}N_{24}C_{18})(34)+\tau_o(H_{27}C_{26}N_{24}C_{18})(12)+\tau_o(H_{19}C_{26}N_{24}C_{18})(12)$
75	214.53		209.96	203.22	$\tau_o(H_{22}C_{20}C_{18}C_{15})(66)+\tau(H_{28}C_{26}N_{24}C_{18})(15)$
76	189.16	152.78	182.67	176.81	$\gamma(C_{18}C_{15}C_4)(19)+\tau_o(C_{15}C_3C_5C_4)(18)+\tau(O_{13}C_2C_6C_1)(15)$
79			115.77	112.05	$\tau_o(H_{12}C_7O_{13}C_2)(22)+\tau_o(C_{17}O_{14}C_1C_2)(57)$
80	83.26	83.25	97.52	94.38	$\tau(C_{18}C_{15}C_4C_3)(64)$
81	61.18	61.18	58.53	56.65	$\beta(C_{18}C_{15}C_4)(22)+\tau_o(C_{15}C_3C_5C_4)(44)$
82			47.07	45.56	$\gamma(C_2C_1C_6)(10)+\tau_o(C_{26}N_{24}C_{18}C_{15})(69)$
83			39.27	38.01	$\tau(N_{24}C_{18}C_{15}C_4)(79)$

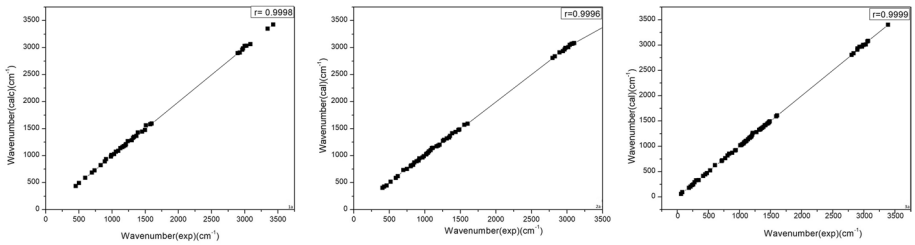

Fig. 9 Correlation graph of calculated and experimental IR spectra of amphetamine (1(**a**)), methamphetamine (2(**a**)), and MDMA (3(**a**))

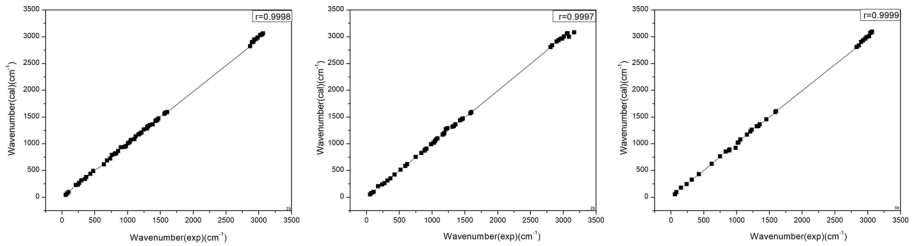

Fig. 10 Correlation graph of calculated and experimental Raman spectra of amphetamine (1(**a**)), methamphetamine (2(**a**)), and MDMA (3(**a**))

of$H_{11}C_7O_{13}C_2$ and that appears at 1346/1344 cm^{-1} in the experimental/calculated IR spectrum of MDMA is assigned to O-C stretch modes

1000-0 cm^{-1}

In this region, the stretching, bending, and torsional modes of C-C, N-C, and O-C are predicted. For amphetamine, the torsional modes corresponding to $H_8C_3C_4C_5$, $H_9C_4C_3C_2$, $H_{11}C_6C_1C_{12}$, $H_{13}C_{12}C_1C_6$, and $H_7C_2C_3C_4$ appear at 978, 960, 893, 855, and 698 cm^{-1} in the experimental spectrum and at 958, 939, 889, 864, and 685 cm^{-1} in the theoretical spectrum. The IR spectrum of methamphetamine shows bands at 970, 923, and 836 cm^{-1}, which are assigned to the torsional modes of $H_9C_3C_4C_5$, $H_8C_2C_3C_4$, and $H_7C_1C_2C_3C_4$, respectively, with corresponding calculated frequencies of 965, 945, and 826 cm^{-1}. In the vibrational spectrum of MDMA, some additional peaks near 1000 cm^{-1} may be due to the stretch and bend modes of O-C. The ring bends, which are a characteristic feature of benzene-type rings used to distinguish the type of substitution, are observed in all three molecules [66]. The ring bend at 597/638 cm^{-1} in the IR/Raman experimental spectrum and 589/613 cm^{-1} in the theoretical spectrum of amphetamine is assigned to the bending modes of $C_1C_6C_5$ and $C_2C_3C_4$, respectively. For methamphetamine, the ring bend at 621/618 cm^{-1} in the experimental/theoretical spectrum is assigned to $C_2C_1C_6$, and for MDMA, the ring bend corresponding to $C_3C_2C_1$ appears at 715 cm^{-1} in the experimental IR spectrum and at 707.55 cm^{-1} in the theoretical spectrum.

Statistical methods were employed to compare the calculated and experimental spectra quantitatively, utilizing the Pearson correlation coefficient as a measure of the

linear correlation between the data sets. This coefficient is a common tool in the analysis of IR and Raman spectra [67]. The correlation results are illustrated in Figs. 9 and 10 demonstrating a robust correlation ($R > 0.9996$) between the experimental and calculated spectral values for all three molecules.

Conclusions

The density functional theory calculations of amphetamine, methamphetamine, and MDMA offered valuable insights into the molecular and electronic properties of these psychoactive compounds. Molecular descriptors such as ionization potential, electron affinity, chemical potential, chemical hardness, chemical softness, electronegativity, electrophilicity index, dipole moment, energy gap, and polarizability were determined using finite difference approximation methods. These descriptors hold significant importance in pharmacological activity and are instrumental in quantitative structure-activity relationship (QSAR) studies and drug design.

The dipole moment and polarizability provide insights into the charge distribution within the molecules, impacting solvation and membrane permeability. Our findings suggest that while the three compounds share similar electronic structures, significant differences exist in their molecular geometries and charge distributions. The calculated values align with the observed properties of Amphetamine, Methamphetamine, and MDMA. Literature suggests that decreased polarity and increased polarizability enhance brain penetration. Consequently, Methamphetamine and MDMA exhibit greater brain penetration compared to Amphetamine, consistent with experimental results. Electron affinity aids in investigating optimal bio availability, while ionization potential is related to blood-brain barrier permeation. Notably, MDMA displays the lowest ionization potential among the three, indicative of its high blood-brain barrier penetration ability. Although the dipole moments of these molecules are low and comparable, their relatively small size suggests a good capacity to penetrate the blood-brain barrier. Ligand binding to an active receptor pocket depends on the ligand's electronic structure, with contributions from dipole moment and polarizability, owing to the strong interaction with the receptor's electrostatic field.

Analysis using Electron Localization Function (ELF) and Non-Covalent Interaction (NCI) reveals both covalent and non-covalent interaction regions within the molecules. Natural Bond Orbital (NBO) analysis indicates that strong hyper conjugative interactions are concentrated on the ring, enhancing biological activity. Among these, MDMA's NBOs demonstrate the highest hyper conjugative interaction, with a stabilization energy of 225 kcal/mol attributed to the methylenedioxy groups. The vibrational analysis (FT-IR and FT-Raman) of these molecules has been conducted both experimentally and theoretically. The obtained wave numbers were analyzed and compared with PED assignments. A quantitative spectral comparison was also performed using linear correlation methods, revealing excellent agreement between the theoretical and experimental data.

Overall, our study highlights the importance of computational methods in understanding the molecular and electronic properties of psychoactive compounds. These findings could have implications for the development of more effective and safer

treatments for psychiatric disorders and substance abuse. Further experimental studies are needed to validate our theoretical predictions and to fully understand the complex pharmacological properties of these compounds. The metabolic products of these drugs are also having a distinct role in their net biological activity. Some of them are more potent than the parent molecule itself. Hence, a complete insight of their activity can be obtained only after analyzing the molecular descriptors of their metabolites which is beyond the scope of this study.

Acknowledgements
The authors wish to express their sincere gratitude to the Department of Chemistry, University College, Thiruvananthapuram for providing access to the Gaussian-16 programme. The Authors extend their thanks to Dr. B. Sandhya IPS, Director, Kerala Police Academy and Smt. Latha Devi MA, Director, FSL for their wholehearted support. The authors would also like to acknowledge the State Forensic Science Laboratory, Thiruvananthapuram and Department of Physics, University of Kerala, Kariavattom, Thiruvananthapuram for their assistance in conducting Spectral measurements.

Authors' contributions
The concept was introduced by AB and SP and then discussed and further refined by VM. Instrumental analysis was done by SP. Analysis and interpretation of the data was done by JS and DM. AB drafted the article which was then revised and finalised by SP and VM. JS and DM reviewed the article.

Funding
The authors declare that no funds, grants, or other support were received during the preparation of this manuscript.

Availability of data and materials
Not applicable.

Declarations

Ethics approval and consent to participate
Not applicable.

Competing interests
The authors have no relevant financial or non-financial interests to disclose.

Received: 24 August 2023 Accepted: 2 June 2024
Published online: 19 June 2024

References

1. United Nations Office on Drug & Crime (2013) The challenge of new psychoactive substances, Global SMART Program. https://www.unodc.org/documents/scientific/NPS_Report.pdf. Accessed 12 Feb 2022
2. United Nations Office on Drug & Crime (2021) World drug report. https://www.unodc.org/res/wdr2021/field/WDR21_Booklet_4.pdf. Accessed 12 Feb 2022.
3. Biel J, Bopp B (1978) Amphetamines: structure-activity relationships. In: Leslie L. Iversen, Susan D. Iversen, Solomon H. Snyder (ed) Stimulants. Handbook of psychopharmacology, vol 11. Springer, New York, p 1–39
4. Sherrill LK, Gulley JM (2018) Effects of amphetamine exposure during adolescence on behavior and prelimbic cortex neuronactivity in adulthood. Brain Res 1694:111–120
5. Heal DJ, Smith SL, Gosden J, Nutt DJ (2013) Amphetamine, past and present - apharmacological and clinical perspective. J Psychopharmacol 27:479–496
6. Moszczynska A (2021) Current and emerging treatments for methamphetamine use disorder. Curr Neuropharmacol 19:2077–2091
7. Sessa LH, Nutt D (2019) A review of 3,4-methylenedioxymethamphetamine (mdma)-assisted psychotherapy. Front Psychiatr 10:138 (1-7). https://doi.org/10.3389/fpsyt.2019.00138
8. Glennon RA, Young R, Hauck AE, McKenney JD (1984) Structure-activity studies on amphetamine analogs using drug discrimination methodology. Pharmacol Biochem Behav 21:895–901
9. Kier LB, Hall LH (1977) Structure-activity studies on hallucinogenic amphetamines using molecular connectivity. J Med Chem 20:1631–1636. https://doi.org/10.1021/jm00222a019. PMID: 592329
10. Rolf Willestofte B, Irene S, Peter Cyril W, Salim A (2012) Raman optical activity and raman spectra of amphetamine species–quantum chemical model calculations and experiments. Am J Anal Chem 3:410–421
11. Taplin F, O'Donnell D, Kubic T, Leona M, Lombardi J (2013) Application of raman spectroscopy, surface-enhanced raman scattering (sers), and density functional theory for the identification of phenethylamines. Appl Spectrosc 67:1150–5
12. Ma H, Hou Y, Fang H, Sarkar A (2021) Investigation of the interaction of amphetamine drug with zn12o12 nanocage: a quantum chemical study. J Comput Electron 20
13. Li X, Jiao X, Li H, Derakhshandeh M (2021) Amphetamine drug detection with inorganic mgo nanotube based on the dft calculations. Appl Biochem Biotechnol 193:3528–3539

14. Bader R, Bader R (1990) Atoms in Molecules: A Quantum Theory In: International Series of Monographs on Chemistry, vol 22. Clarendon Press, Oxford. https://books.google.co.in/books?id=up1pQgAACAAJ
15. Lu T, Chen F (2012) Multiwfn: A multifunctional wavefunction analyzer. J Comput Chem 33:580–92
16. Frisch MJ et al (2016) Gaussian 16 Revision C.01. Gaussian Inc., Wallingford
17. Hohenberg P, Kohn W (1964) Inhomogeneous electron gas. Phys Rev 136:B864–B871. https://link.aps.org/doi/10.1103/PhysRev.136.B864. Accessed 24 Aug 2022.
18. Kohn W, Sham LJ (1965) Self consistent equations including exchange and correlation effects. Phys Rev 140:A1133–A1138. https://link.aps.org/doi/10.1103/PhysRev.140.A1133. Accessed 24 Aug 2022.
19. Lee C, Yang W, Parr RG (1988) Development of the colle-salvetti correlationenergy formula into a functional of the electron density. Phys Rev B 37:785–789. https://link.aps.org/doi/10.1103/PhysRevB.37.785. Accessed 25 Aug 2022.
20. Becke AD (1993) Density-functional thermochemistry. the role of exact exchange. J Chem Phys 98:5648–5652. https://doi.org/10.1063/1.464913
21. Parr RG, Yang W (1989) Density-functional theory of atoms and molecules. Oxford University Press, New York
22. Jamroz MH (2013) Vibrational energy distribution analysis (VEDA): Scopes and limitations. Spectrochim Acta A Mol Biomol Spectrosc 114:220–230. https://doi.org/10.1016/j.saa.2013.05.096
23. Jamroz MH (2004) Vibrational Energy Distribution Analysis VEDA 4. Warsaw
24. Parr RG, Lv Szentpály, Liu S (1999) Electrophilicity index. J Am Chem Soc 121:1922–1924. https://doi.org/10.1021/ja983494x
25. Hehre J, Radom L, Schleyer PVR, Pople JA (1986) Ab initio Molecular Orbital theory. Wiley Newyork
26. Jane M, Peter P (2011) The electrostatic potential: an overview. Comput Mol Sci 1:153–163
27. Parr RG, Pearson RG (1983) Absolute hardness: companion parameter to absolute electronegativity. J Am Chem Soc 105:7512–7516. https://doi.org/10.1021/ja00364a005
28. Geerlings P, De Proft F, Langenaeker W (2003) Conceptual density functional theory. Chem Rev 103:1793–1874. https://doi.org/10.1021/cr990029p. PMID: 12744694
29. Fleming I (1976) Frontier orbitals and organic chemical reactions. Wiley
30. Aihara J-i (1999) Reduced homo lumo gap as an index of kinetic stability for polycyclic aromatic hydrocarbons. J Phys Chem A 103:7487–7495. https://doi.org/10.1021/jp990092i
31. Pearson RG (1993) The principle of maximum hardness. Acc Chem Res 26:250–255. https://doi.org/10.1021/ar00029a004
32. Kumar VRL, Kishor S (2013) Understanding the antioxidant behavior of some vitamin molecules: a first-principles density functional approach. J Mol Model 19:3175–86
33. Parr RG, Yang W (1984) Density functional approach to the frontier-electron theory of chemical reactivity. J Am Chem Soc 106:4049–4050. https://doi.org/10.1021/ja00326a036
34. Kaya S, Kaya C (2015) A new equation for calculation of chemical hardness of groups and molecules. Mol Phys 113:1311–1319. https://doi.org/10.1080/00268976.2014.991771
35. Islam N, Ghosh DC (2011) Spectroscopic evaluation of the global hardness of the atoms. Mol Phys 109:1533–1544
36. Pearson RG (1963) Hard and soft acids and bases. J Am Chem Soc 85:3533–3539. https://doi.org/10.1021/ja00905a001
37. Pearson RG (1966) Acids and bases: Hard acids prefer to associate with hard bases, and soft acids prefer to associate with soft bases. Science 151:172–177
38. Hassan Baig M et al (2016) Computer aided drug design: success and limitations. Curr Pharm Des 22:572–581
39. Semeniuk A, Kalinowska-Tluscik J, Nitek W, Oleksyn BJ (2008) Intermolecular interactions in crystalline hydroxychloroquine sulfate in comparison with those in selected antimalarial drugs. J Chem Crystallogr 38:333–338
40. Biel J (1970) Structure-activity relationships of amphetamine and derivatives. Amphetamines Relat Compd 3–19
41. LaPointe SM, Weaver DF (2007) A review of density functional theory quantum mechanics as applied to pharmaceutically relevant systems. Curr Comput Aided Drug Des 3:290–296
42. Becke AD, Edgecombe KE (1990) A simple measure of electron localization in atomic and molecular systems. J Chem Phys 92:5397–5403. https://doi.org/10.1063/1.458517
43. Silvi B, Savin A (1994) Classification of chemical bonds based on topological analysis of electron localization functions. Nature 371:683–86
44. Johnson ER et al (2010) Revealing noncovalent interactions. J Am Chem Soc 132:6498–6506. https://doi.org/10.1021/ja100936w. (PMID: 20394428)
45. LU T, CHEN F-W (2011) Meaning and functional form of the electron localization function. Acta Phys Chim Sin 27:2786. http://www.whxb.pku.edu.cn/EN/abstract/article 27788.shtml
46. Cao J, Ren Q, Chen F, Lu T (2015) Comparative study on the methods for predicting the reactive site of nucleophilic reaction. Sci China Chem 58:1845–1852
47. Yang W, Mortier WJ (1986) The use of global and local molecular parameters for the analysis of the gas-phase basicity of amines. J Am Chem Soc 108(19):5708–11. https://doi.org/10.1021/ja00279a008. Accessed 9 Oct 2022.
48. Morell C, Grand A, Toro-Labbé A (2005) New dual descriptor for chemical reactivity. J Phys Chem A 109:205–12
49. Politzer P, Laurence PR, Jayasuriya K (1985) Molecular electrostatic potentials: an effective tool for the elucidation of biochemical phenomena. Environ Health Perspect 61:191–202
50. Scrocco E, Tomasi J (2005) In: The electrostatic molecular potential as a tool for the interpretation of molecular properties. Springer, pp 95-170
51. Scrocco E, Tomasi J (1978) Electronic molecular structure, reactivity and intermolecular forces: an euristic interpretation by means of electrostatic molecular potentials. Adv Quantum Chem 11:115–193
52. Glendening ED, Landis CR, Weinhold F (2012) Natural bond orbital methods. Wiley Interdiscip Rev Comput Mol Sci 2:1–42
53. Weinhold F, Carpenter JE (1988) The Structure of Small Molecules and Ions., Ch. The Natural Bond Orbital Lewis Structure Concept for Molecules, Radicals and Radical Ions. Springer, Boston, pp 227-236
54. Reed AE, Curtiss LA, Weinhold F (1988) Intermolecular interactions from a natural bond orbital, donor-acceptor viewpoint. Chem Rev 88:899–926

55. Lionel Goodman RRS (2006) Diffuse functions in natural bond orbital analysis. J Comput Chem 28:269–275
56. Weinhold F, Glendening ED. NBO 7.0 Program Manual Natural Bond Orbital Analysis Programs
57. Kalsi PS (2007) Spectroscopy of organic compounds. New Age International
58. Polavarapu PL (1990) Ab initio vibrational raman and raman optical activity spectra. J Phys Chem 94:8106–8112. https://doi.org/10.1021/j100384a024
59. Andersson M, Uvdal P (2005) New scale factors for harmonic vibrational frequencies using the B3LYP density functional method with the triple-ζ basis set 6-311+G(d,p). J Phys Chem A 109:2937–41. https://doi.org/10.1021/jp045733a
60. Varsányi G, Láng L, Kovner MA, Lempert K. Assignments for vibrational spectra of seven hundred benzene derivatives. Akademiai Kiado, Budapest
61. Socrates G (2004) Infrared and Raman Characteristic Group Frequencies: Tables and Charts, 3rd edn. Wiley
62. Cain BR, Freeman JM, Henshall T (1969) On the characteristic vibrations of the nh2 group. Can J Chem 47:2947
63. Bellamy LJ (1975) The Infra-red spectra of complex molecules. Springer
64. Colthup N et al (1990) Introduction to Infrared and Raman Spectroscopy. Academic Press
65. Srivastava A et al (2017) Spectroscopic (far or terahertz, mid-infrared and raman) investigation, thermal analysis and biological activity of piplartine. Spectrochim Acta A Mol Biomol Spectrosc 184:368–381. https://www.sciencedirect.com/science/article/pii/S1386142517303748
66. Smith B (2018) Infrared spectral interpretation: a systematic approach. CRC Press
67. Henschel H, Andersson AT, Jespers W, Mehdi Ghahremanpour M, Van der Spoel D (2020) Theoretical infrared spectra: quantitative similarity measures and force fields. J Chem Theory Comput 16:3307–3315

Publisher's Note